

On Thinning Ice: Modeling Sea Ice in a Warming Climate

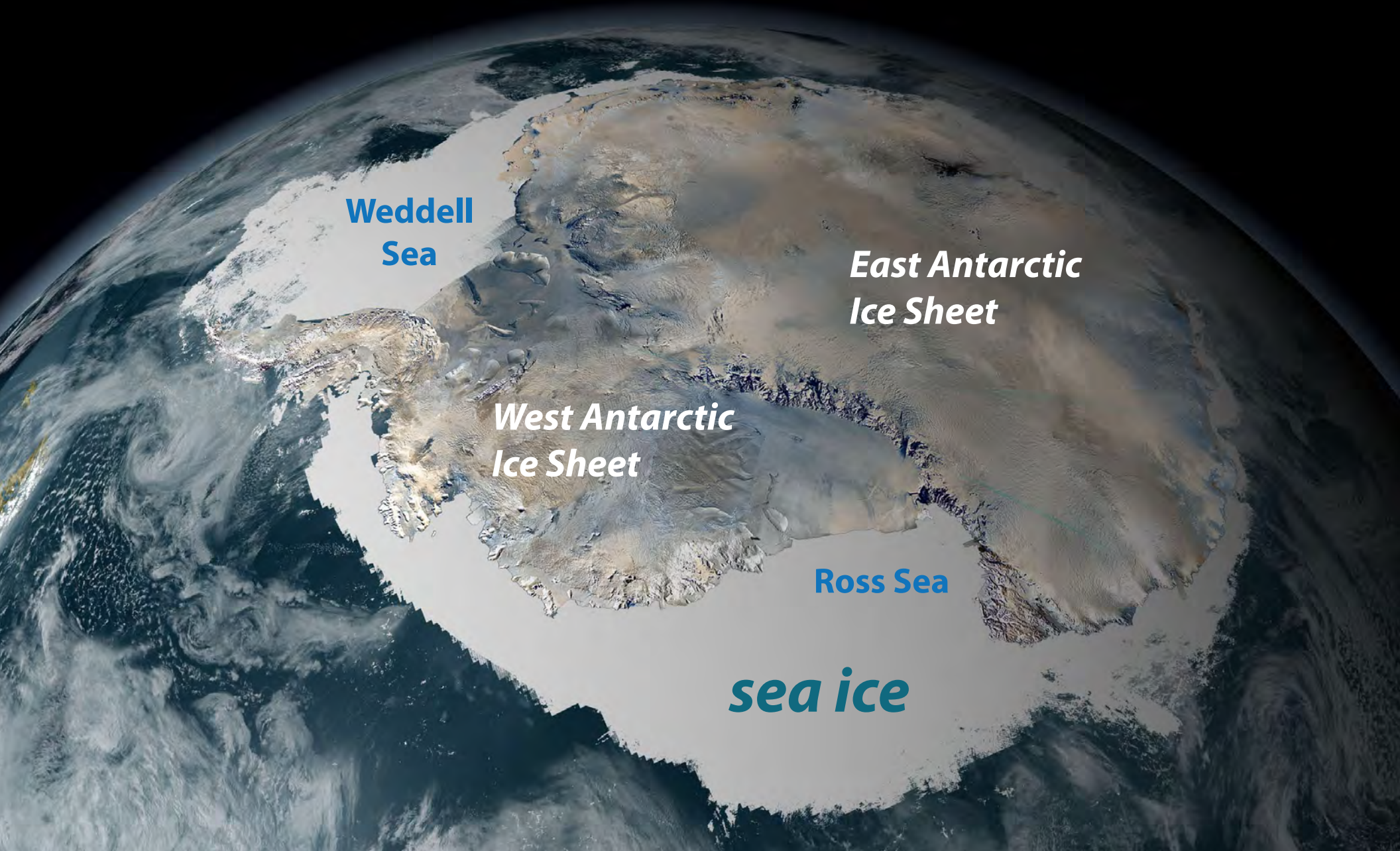
Kenneth M. Golden
Department of Mathematics, University of Utah



Joint ORFE and PACM Colloquium
8 February 2022

ANTARCTICA

southern cryosphere



**Weddell
Sea**

***East Antarctic
Ice Sheet***

***West Antarctic
Ice Sheet***

Ross Sea

sea ice

SEA ICE covers ~12% of Earth's ocean surface

- boundary between ocean and atmosphere
- mediates exchange of heat, gases, momentum
- global ocean circulation
- hosts rich ecosystem
- indicator of **climate change**



polar ice caps critical to global climate in reflecting incoming solar radiation



white snow and ice
reflect

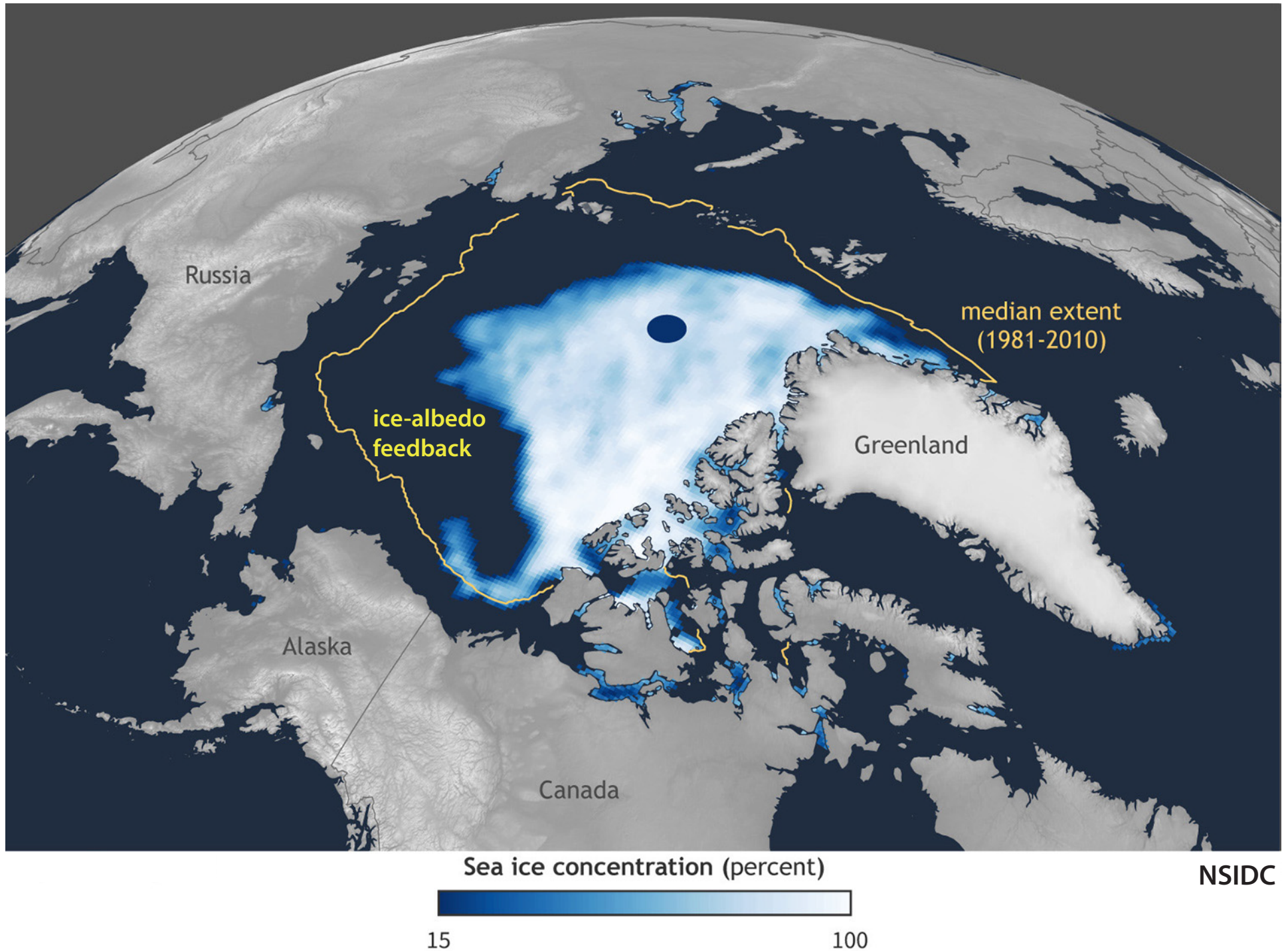


dark water and land
absorb

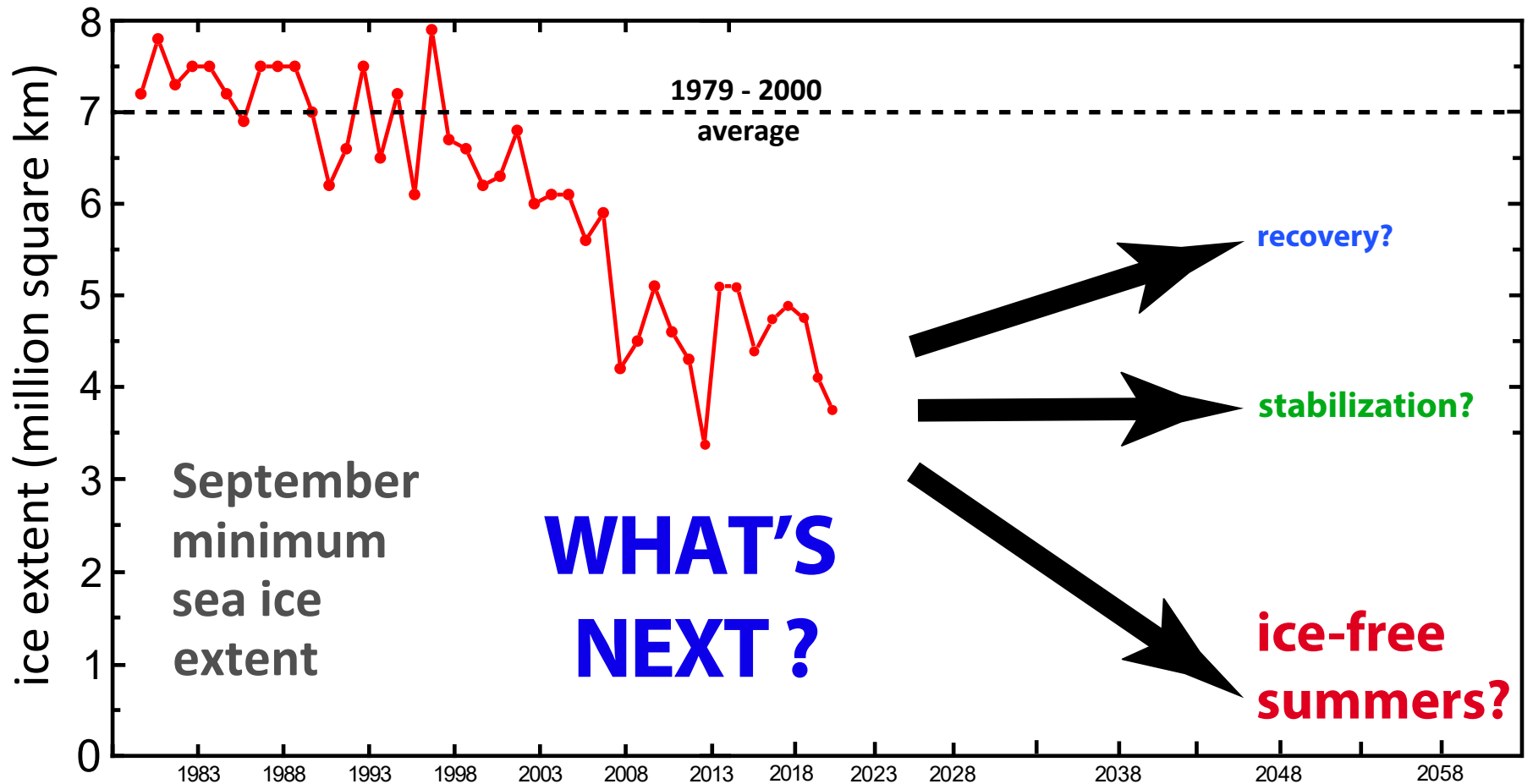
$$\text{albedo } \alpha = \frac{\text{reflected sunlight}}{\text{incident sunlight}}$$

Arctic sea ice extent

September 15, 2020



Predicting what may come next requires lots of math modeling.



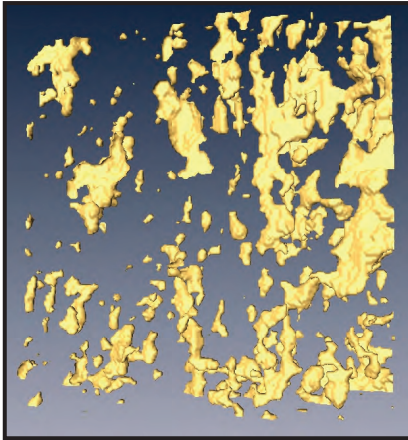
Sea Ice is a Multiscale Composite Material

microscale

brine inclusions

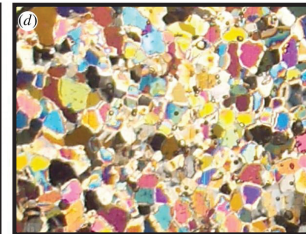
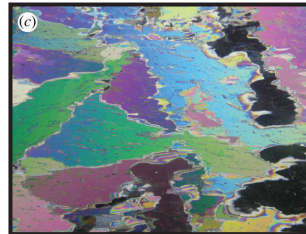
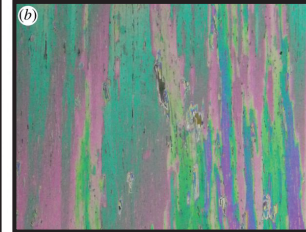


Weeks & Assur 1969



H. Eicken
Golden et al. GRL 2007

polycrystals

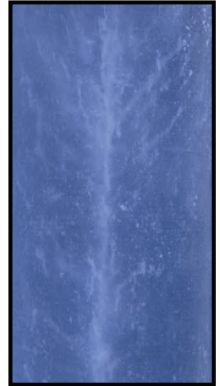


Gully et al. Proc. Roy. Soc. A 2015

brine channels



D. Cole



K. Golden

millimeters

centimeters

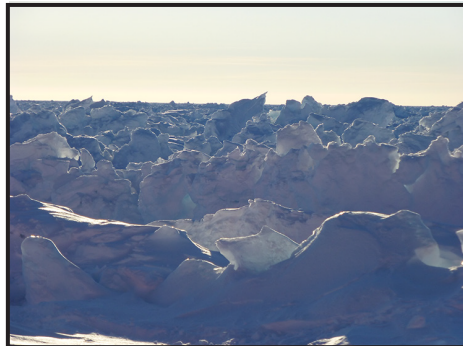
mesoscale

Arctic melt ponds



K. Frey

Antarctic pressure ridges



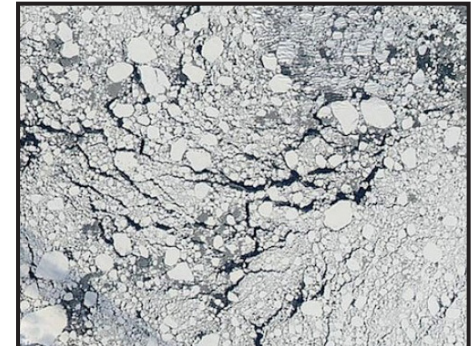
K. Golden

sea ice floes



J. Weller

sea ice pack



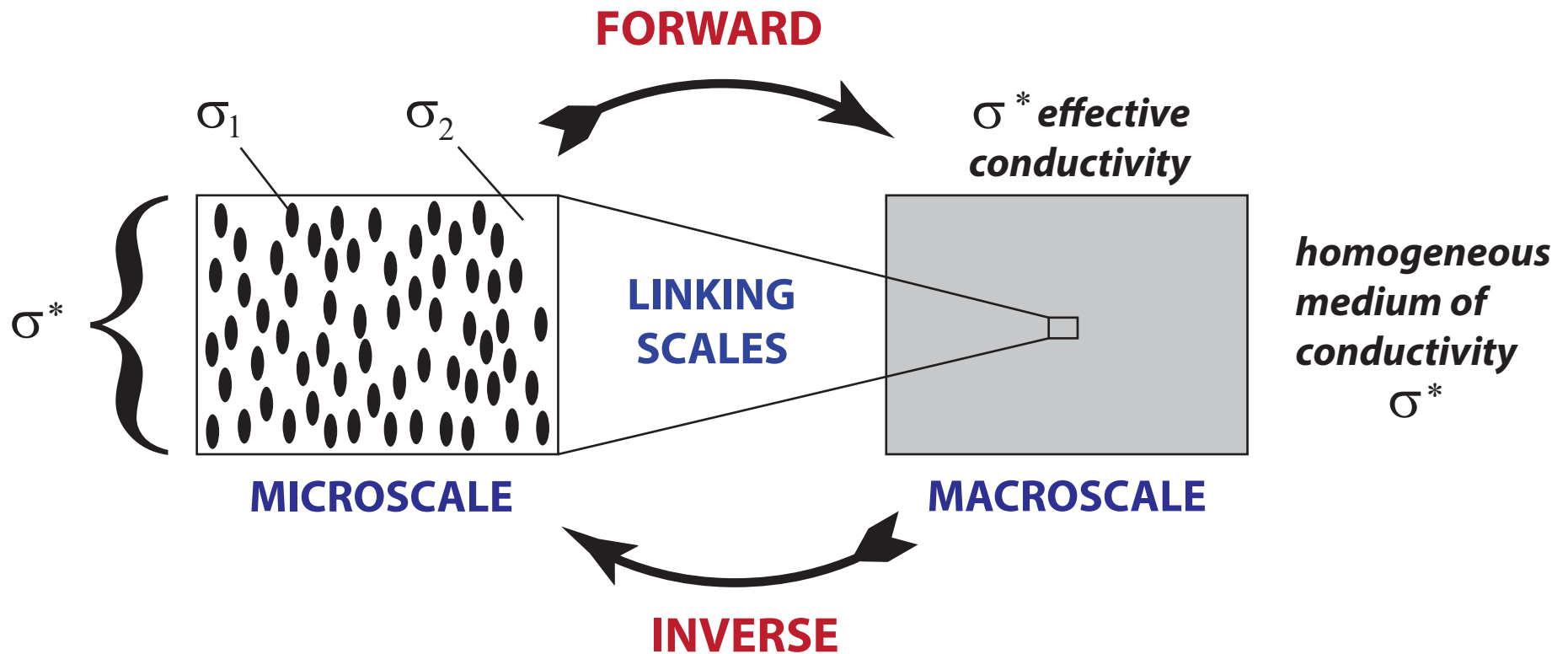
NASA

meters

kilometers

macroscale

HOMOGENIZATION for Composite Materials



Maxwell 1873 : effective conductivity of a dilute suspension of spheres

Einstein 1906 : effective viscosity of a dilute suspension of rigid spheres in a fluid

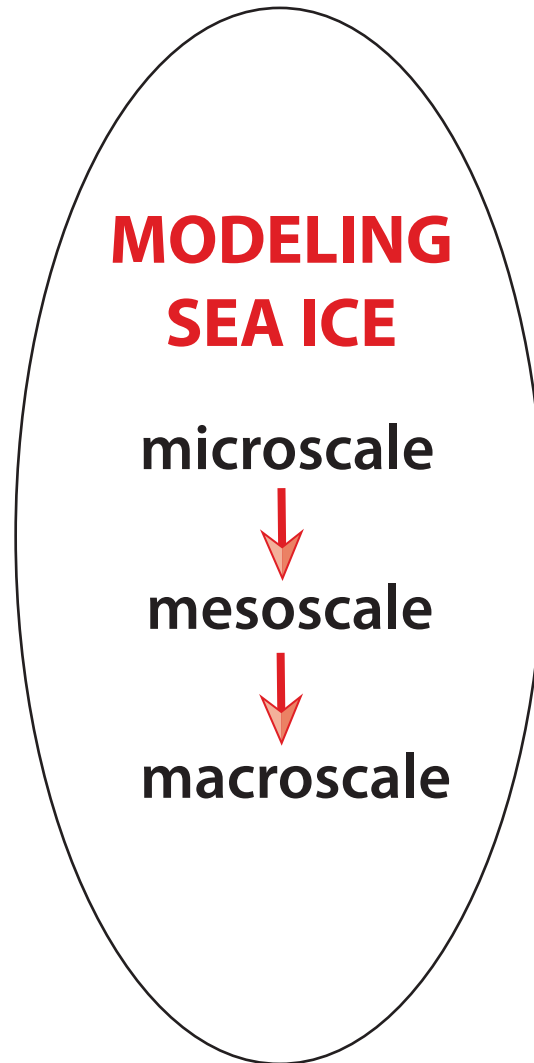
*Wiener 1912 : arithmetic and harmonic mean **bounds** on effective conductivity*

*Hashin and Shtrikman 1962 : variational **bounds** on effective conductivity*

widespread use of composites in late 20th century due in large part to advances in mathematically predicting their effective properties

What is this talk about?

Using methods of **homogenization and statistical physics** to model sea ice effective behavior and advance representation of sea ice in climate models, process studies, ...



A tour of key sea ice processes on micro, meso, and macro scales.

What is our research about?

Using methods of **homogenization and statistical physics** to model sea ice effective behavior and advance representation of sea ice in climate models, process studies, ...

Inputs, Ingredients

COMPOSITE MATERIALS

electrical engineering,
stealth technology

porous media,
oil extraction

statistical mechanics
of ferromagnets

Anderson localization,
semiconductor physics

random matrix theory

differential equations



MODELING SEA ICE

microscale

mesoscale

macroscale

Outputs, Impacts

CLIMATE MODELING

sea ice physics
& biology

composites,
polycrystals

remote sensing

advection diffusion

biomedical imaging,
biomaterials, EPS

polar microbial ecology



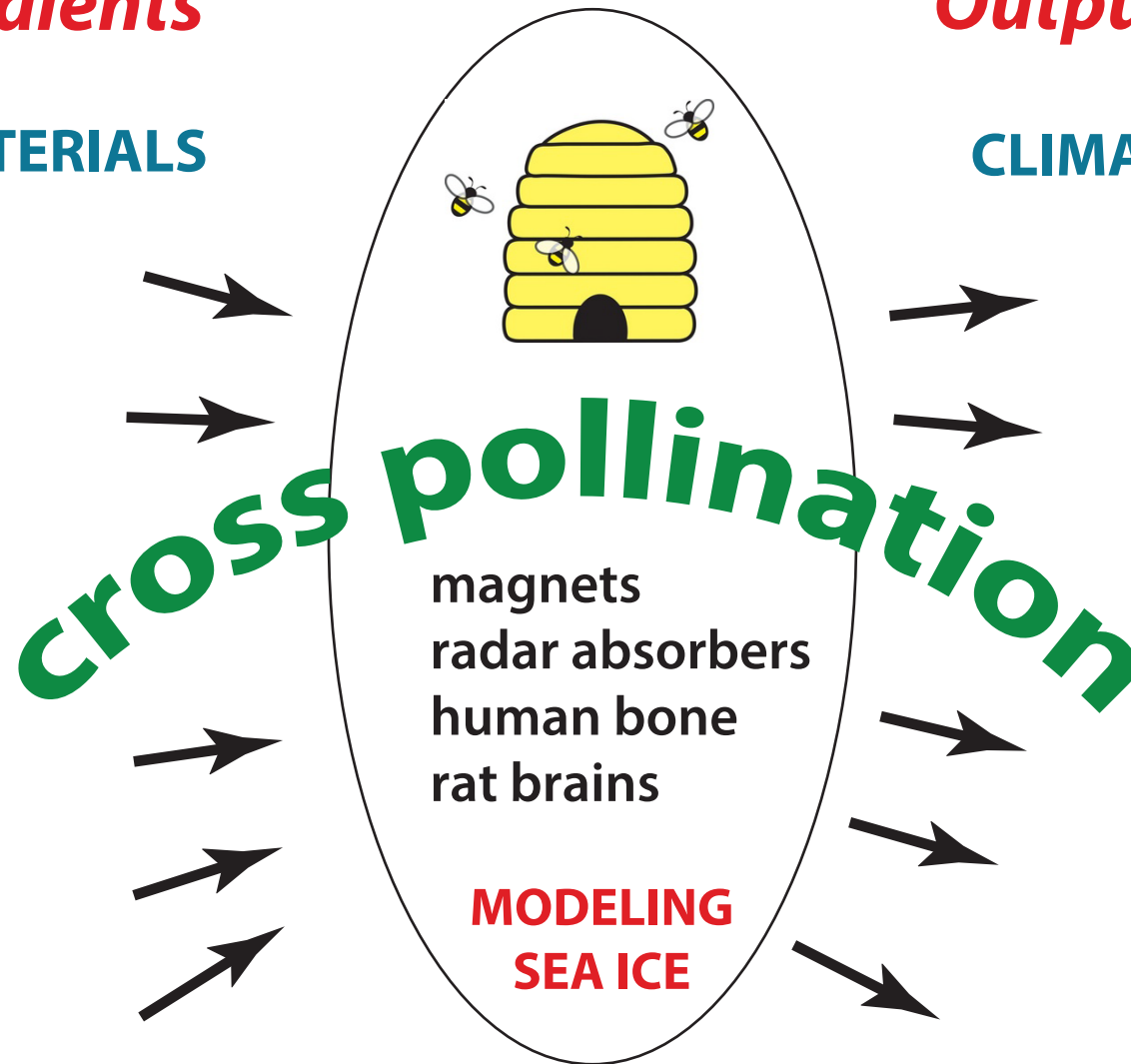
What is our research about?

Inputs, Ingredients

COMPOSITE MATERIALS

Outputs, Impacts

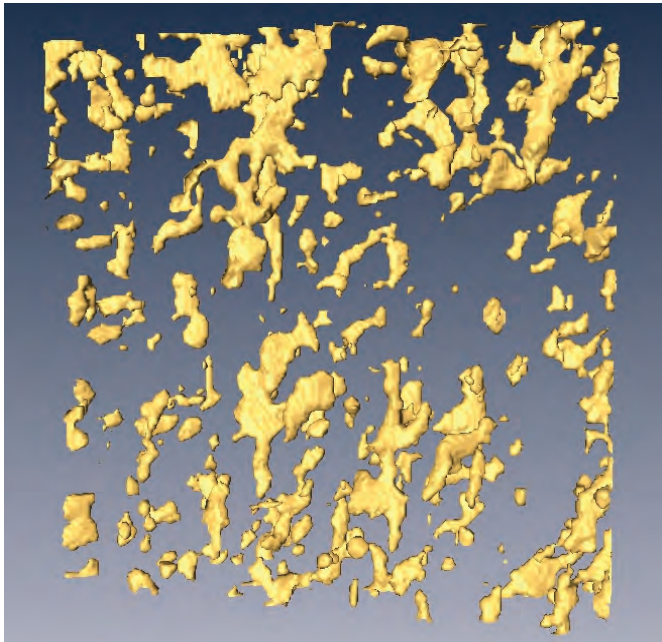
CLIMATE MODELING



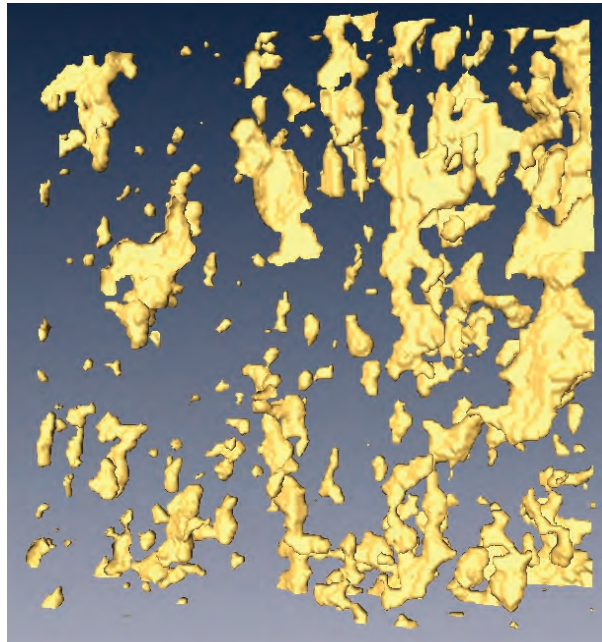
Modeling sea ice drives advances in many areas of science and engineering.

microscale

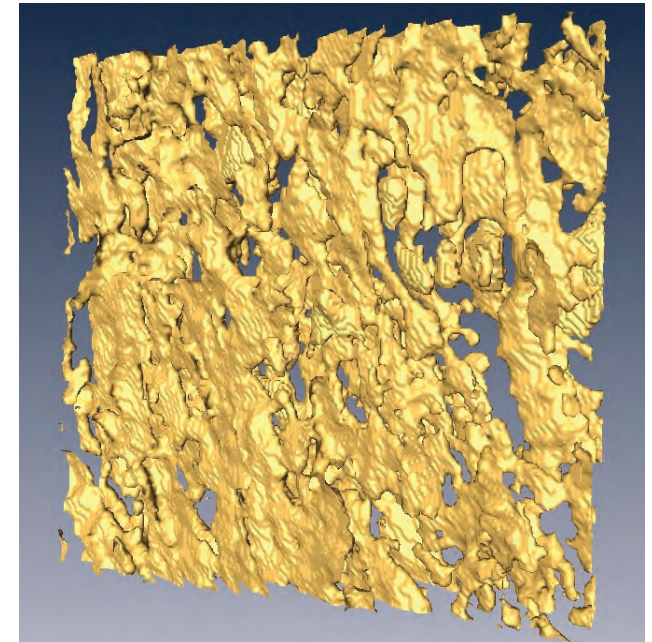
brine volume fraction and **connectivity** increase with temperature



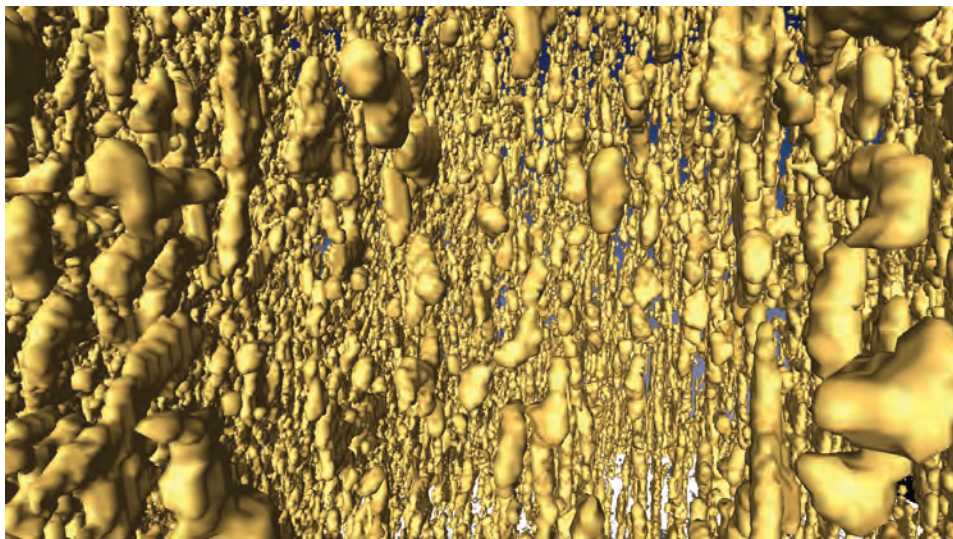
$T = -15\text{ }^{\circ}\text{C}$, $\phi = 0.033$



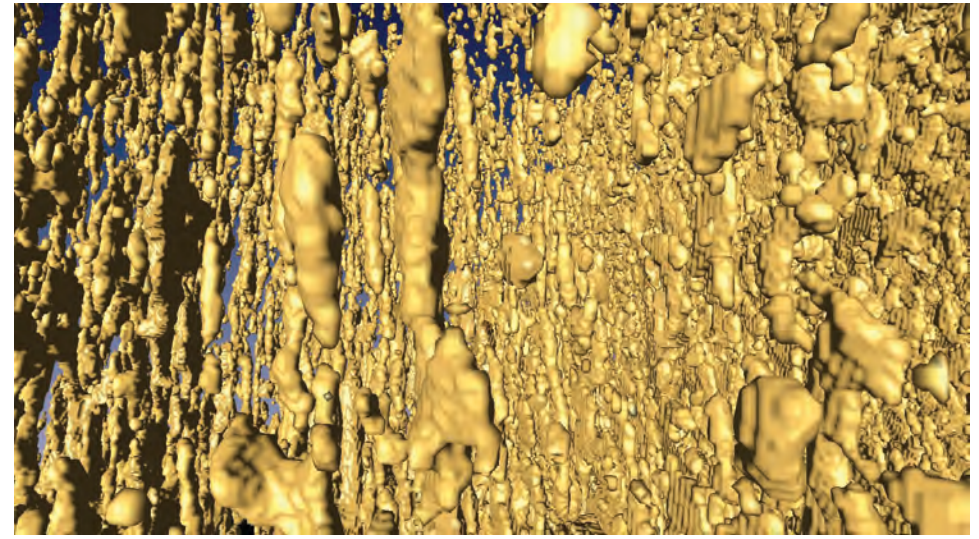
$T = -6\text{ }^{\circ}\text{C}$, $\phi = 0.075$



$T = -3\text{ }^{\circ}\text{C}$, $\phi = 0.143$



$T = -8\text{ }^{\circ}\text{C}$, $\phi = 0.057$



$T = -4\text{ }^{\circ}\text{C}$, $\phi = 0.113$

X-ray tomography for brine in sea ice

Golden et al., *Geophysical Research Letters*, 2007

fluid flow through the porous microstructure of sea ice governs key processes in polar climate and ecosystems

evolution of Arctic melt ponds and sea ice albedo



nutrient flux for algal communities



T. Maksym and T. Markus, 2008

*Antarctic surface flooding
and snow-ice formation*

September
snow-ice
estimates

- evolution of salinity profiles
- ocean-ice-air exchanges of heat, CO_2

fluid permeability of a porous medium



how much water gets through the sample per unit time?

Darcy's Law

for slow viscous flow in a porous medium

averaged
fluid velocity

pressure
gradient

$$\mathbf{v} = -\frac{\mathbf{k}}{\eta} \nabla p$$

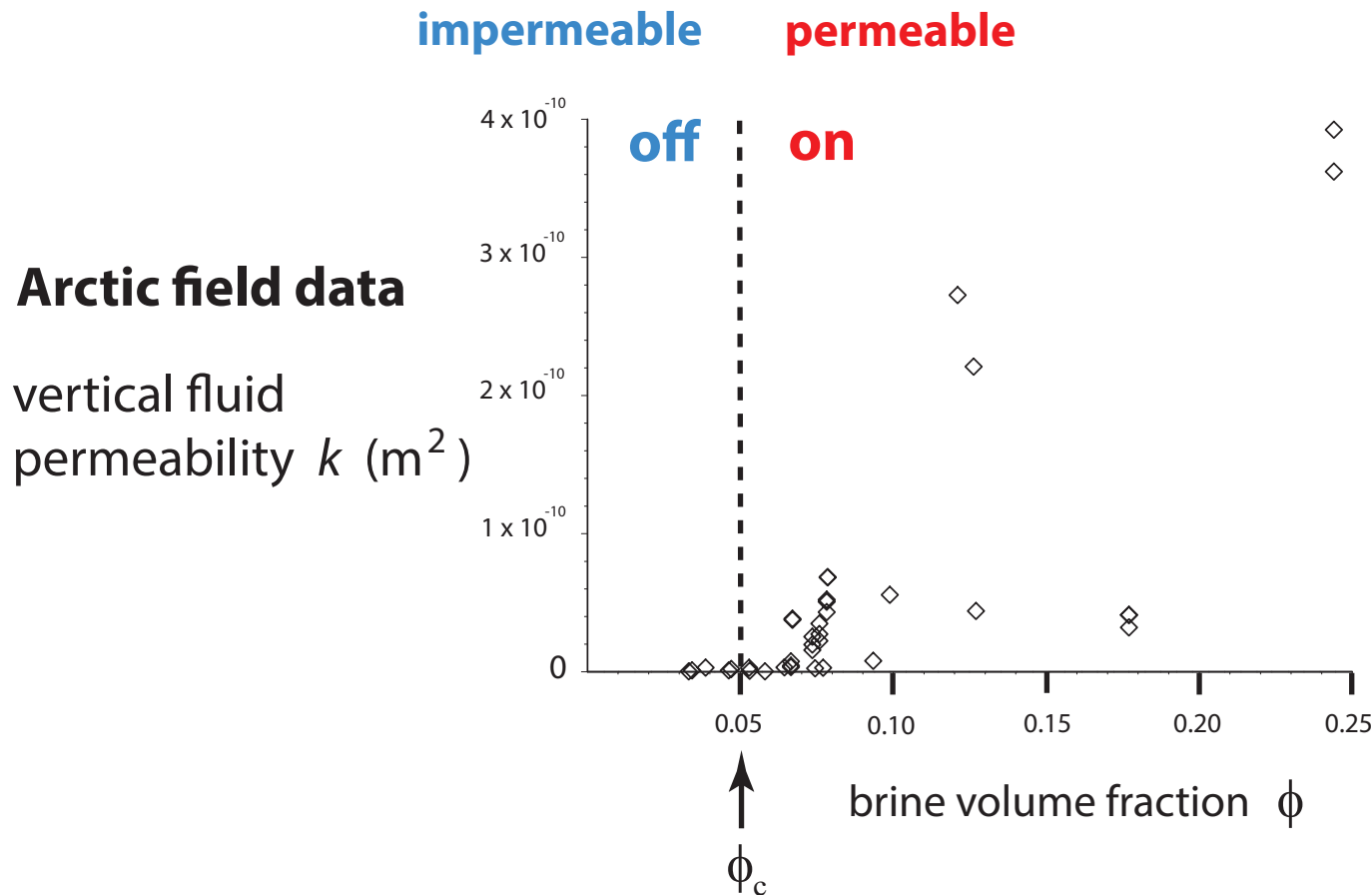
viscosity

\mathbf{k} = fluid permeability tensor

HOMOGENIZATION

mathematics for analyzing effective behavior of heterogeneous systems

Critical behavior of fluid transport in sea ice



***“on - off” switch
for fluid flow***

critical brine volume fraction $\phi_c \approx 5\% \longleftrightarrow T_c \approx -5^\circ \text{C}, S \approx 5 \text{ ppt}$

RULE OF FIVES

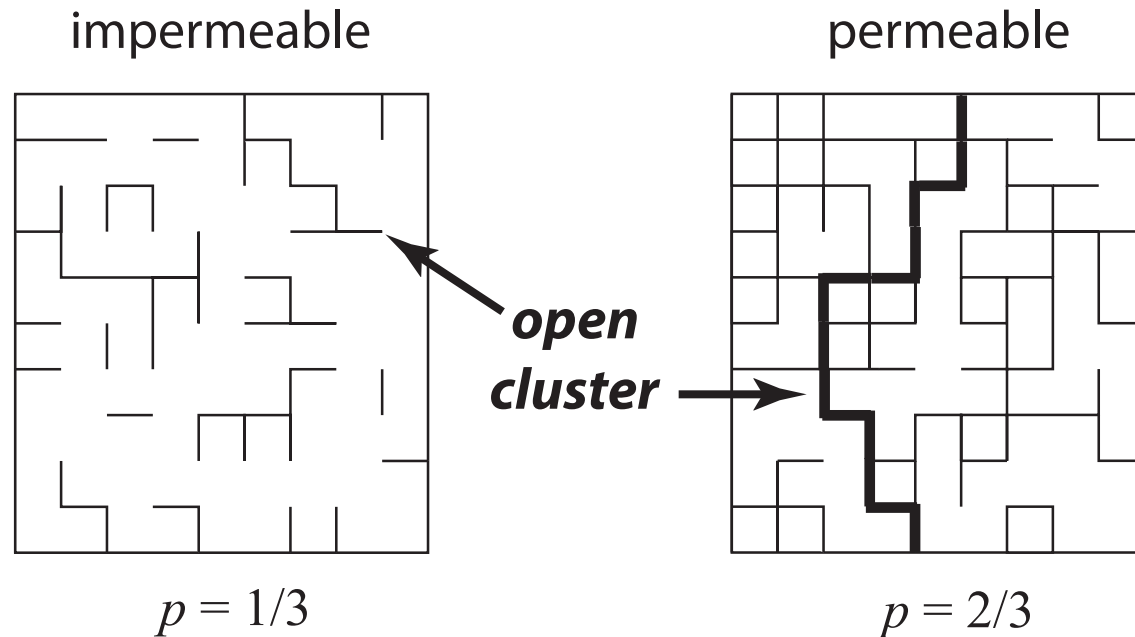
Golden, Ackley, Lytle Science 1998

Golden, Eicken, Heaton, Miner, Pringle, Zhu GRL 2007

Pringle, Miner, Eicken, Golden J. Geophys. Res. 2009

percolation theory

probabilistic theory of connectedness



bond \longrightarrow *open* with probability p
closed with probability $1-p$

percolation threshold

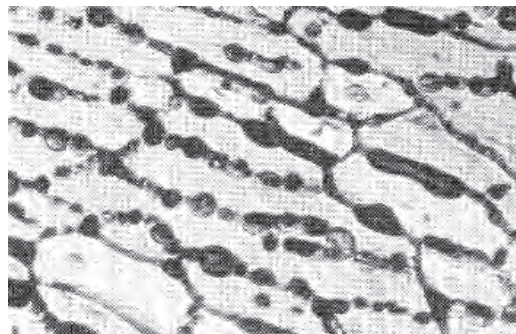
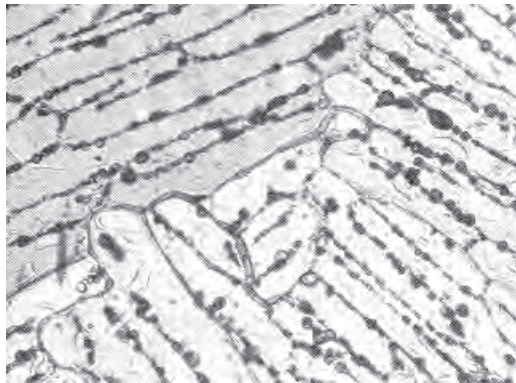
$$p_c = 1/2 \quad \text{for } d = 2$$

smallest p for which there is an infinite open cluster

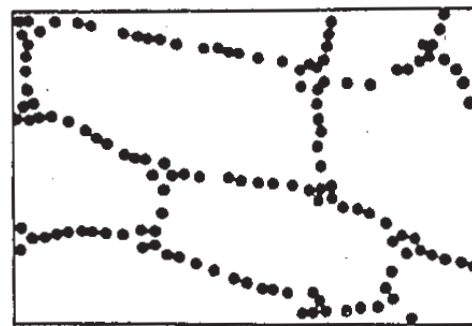
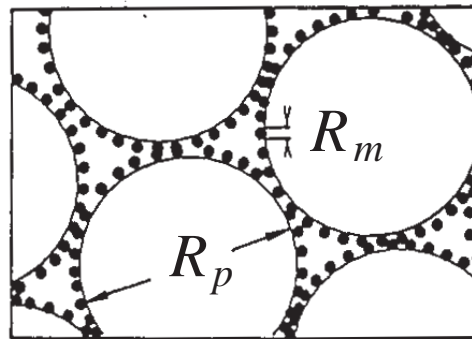
Continuum percolation model for **stealthy** materials applied to sea ice microstructure explains **Rule of Fives** and Antarctic data on **ice production** and **algal growth**

$$\phi_c \approx 5 \%$$

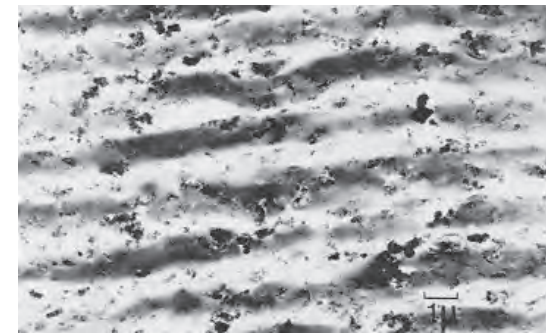
Golden, Ackley, Lytle, *Science*, 1998



sea ice



compressed
powder

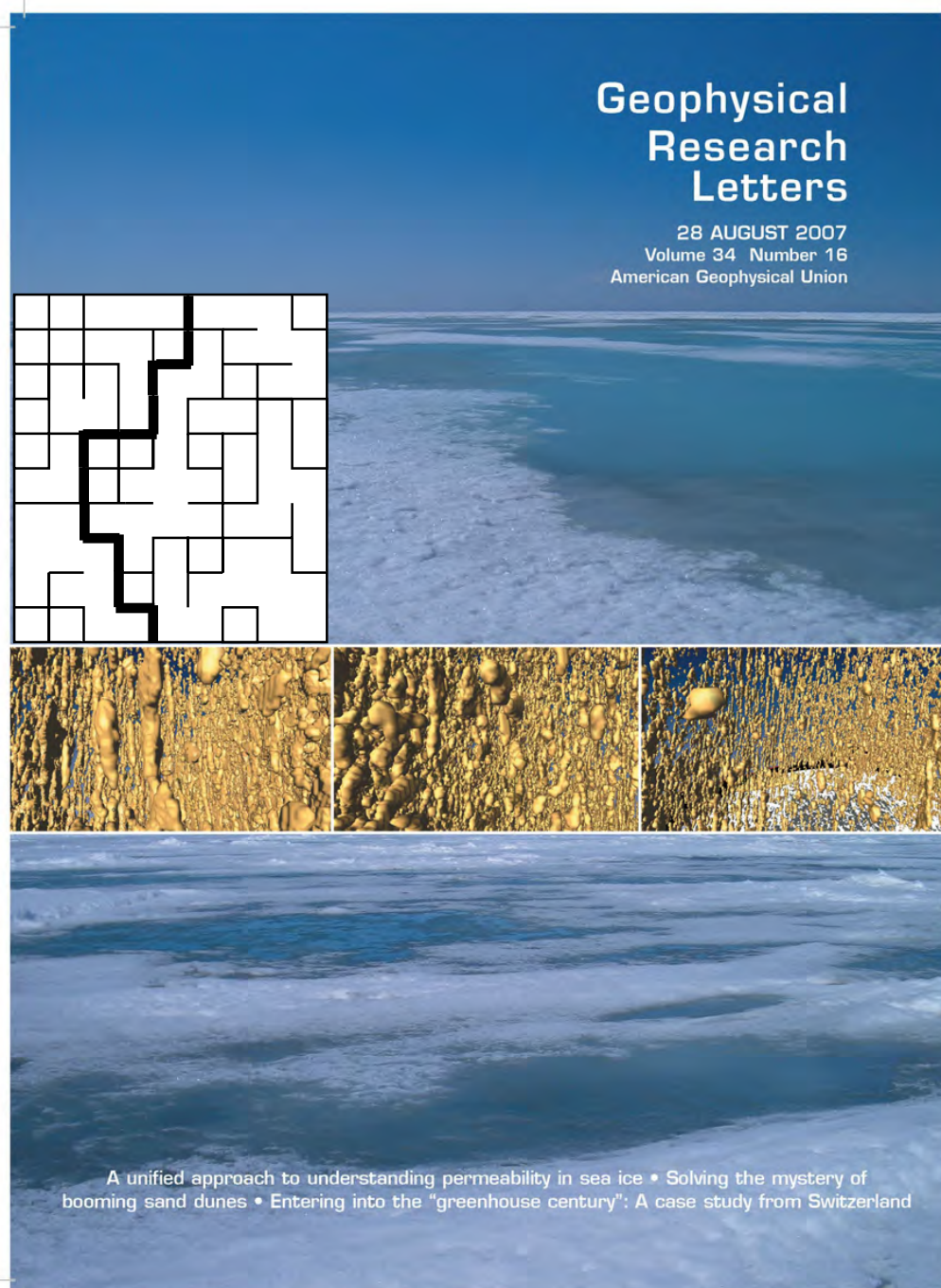


radar absorbing
composite

sea ice is radar absorbing

Thermal evolution of permeability and microstructure in sea ice

Golden, Eicken, Heaton*, Miner, Pringle, Zhu, *Geophysical Research Letters* 2007



**percolation theory
for fluid permeability**

$$k(\phi) = k_0 (\phi - 0.05)^2$$

critical
exponent
 t

$$k_0 = 3 \times 10^{-8} \text{ m}^2$$

from critical path analysis
in **hopping conduction**

hierarchical model

rock physics

network model

rigorous bounds

**X-ray tomography for
brine inclusions**

confirms rule of fives

*Pringle, Miner, Eicken, Golden
J. Geophys. Res. 2009*

**theories agree closely
with field data**

microscale
governs

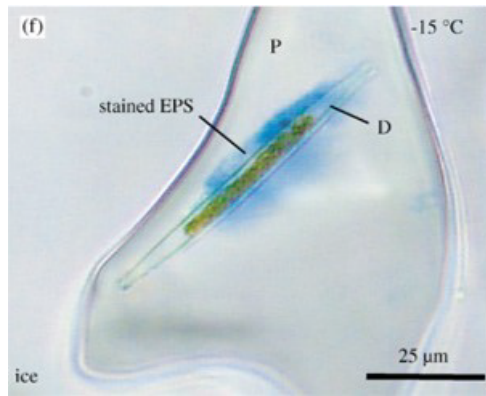
mesoscale
processes

**melt pond
evolution**

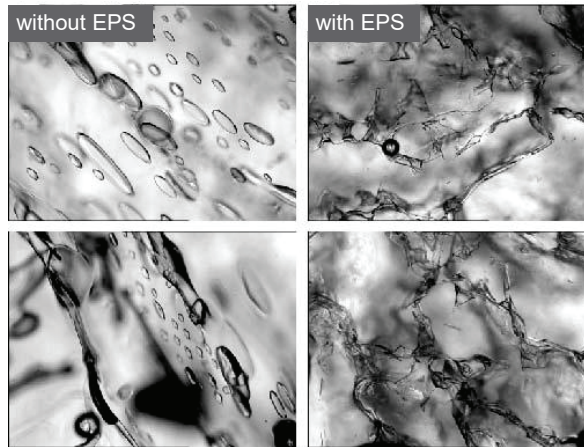
A unified approach to understanding permeability in sea ice • Solving the mystery of
booming sand dunes • Entering into the "greenhouse century": A case study from Switzerland

Sea ice algae secrete extracellular polymeric substances (EPS) affecting evolution of brine microstructure.

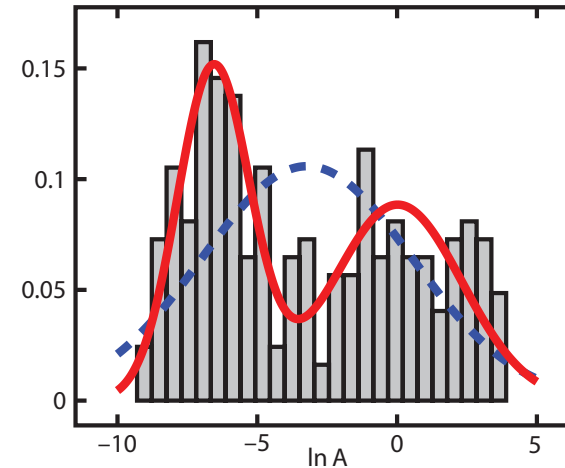
How does EPS affect fluid transport? How does the biology affect the physics?



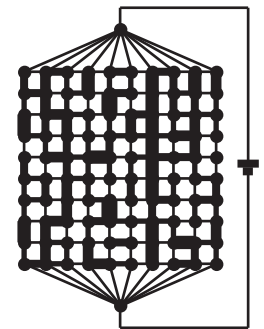
Krembs



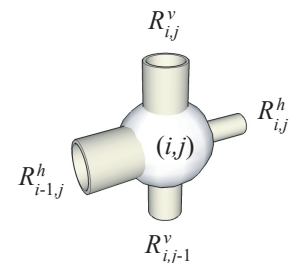
Krembs, Eicken, Deming, PNAS 2011



**RANDOM
PIPE
MODEL**



- 2D random pipe model with bimodal distribution of pipe radii
- Rigorous bound on permeability k ; results predict observed drop in k



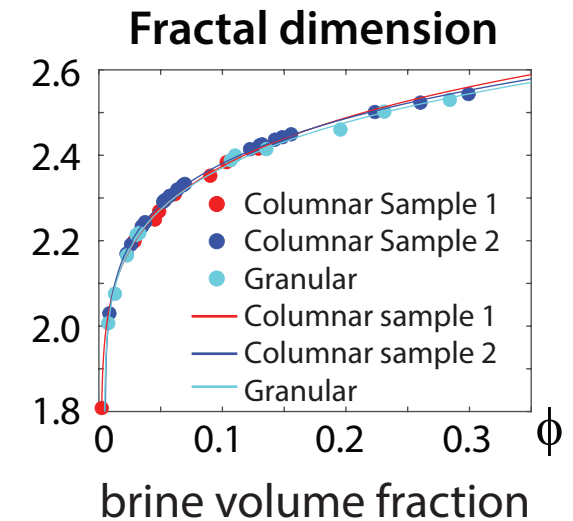
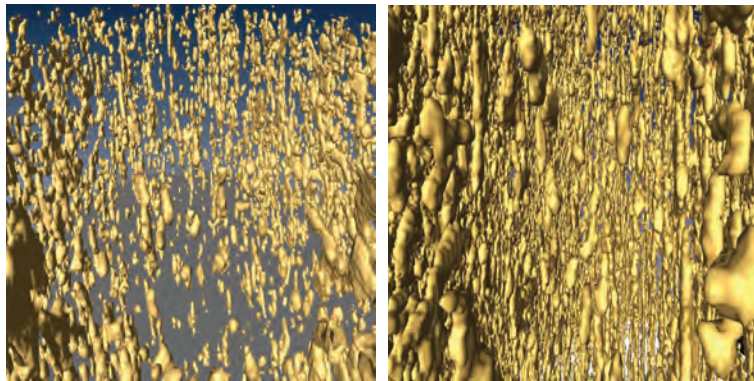
Steffen, Epshteyn, Zhu, Bowler, Deming, Golden
Multiscale Modeling and Simulation, 2018

Zhu, Jabini, Golden,
Eicken, Morris
Ann. Glac. 2006

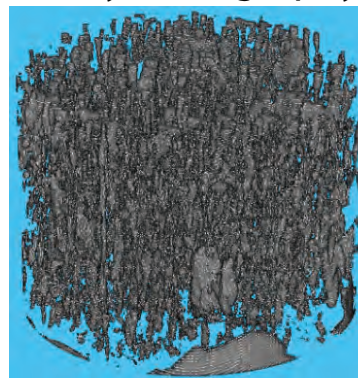
Thermal evolution of the fractal geometry of the brine microstructure in sea ice

N. Ward, D. Hallman, H. Eicken, M. Oggier and K. M. Golden, 2022

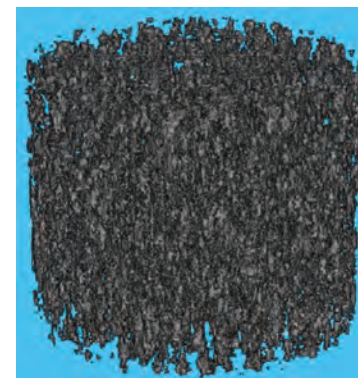
$T = -12\text{ }^{\circ}\text{C}$, $\phi = 0.033$ $T = -8\text{ }^{\circ}\text{C}$, $\phi = 0.057$



X-ray tomography



DLA model



Arctic and Antarctic field experiments

*develop electromagnetic methods
of monitoring fluid transport and
microstructural transitions*

extensive measurements of fluid and
electrical transport properties of sea ice:

2007 Antarctic SIPEX

2010 Antarctic McMurdo Sound

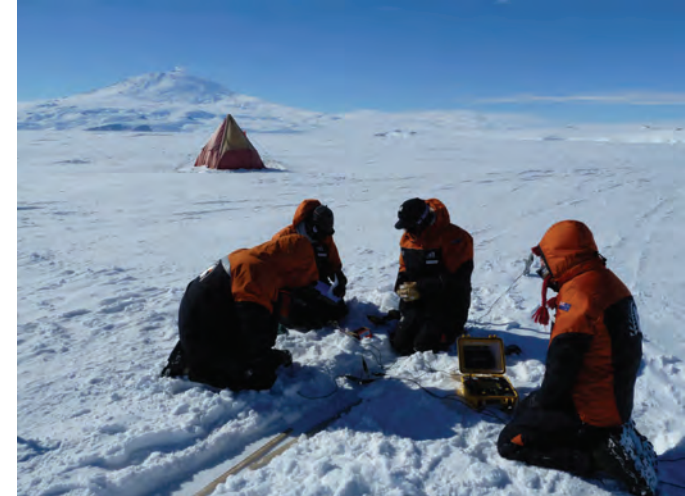
2011 Arctic Barrow AK

2012 Arctic Barrow AK

2012 Antarctic SIPEX II

2013 Arctic Barrow AK

2014 Arctic Chukchi Sea



Notices

of the American Mathematical Society

May 2009

Volume 56, Number 5

Climate Change and
the Mathematics of
Transport in Sea Ice

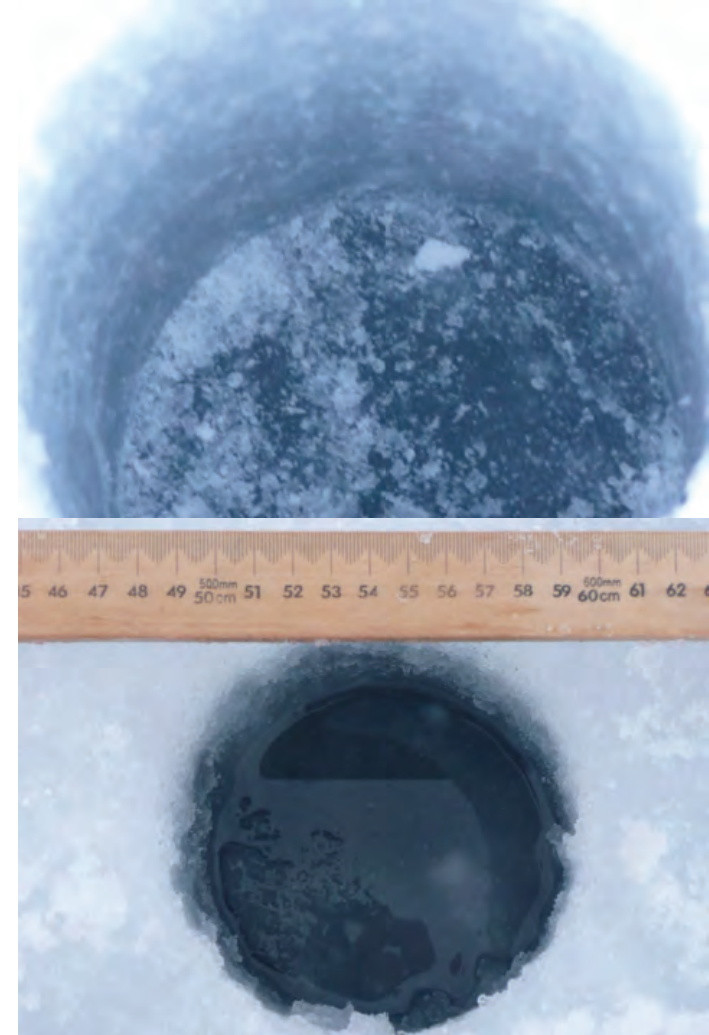
page 562

Mathematics and the
Internet: A Source of
Enormous Confusion
and Great Potential

page 586

photo by Jan Lieser

Real analysis in polar coordinates (see page 613)



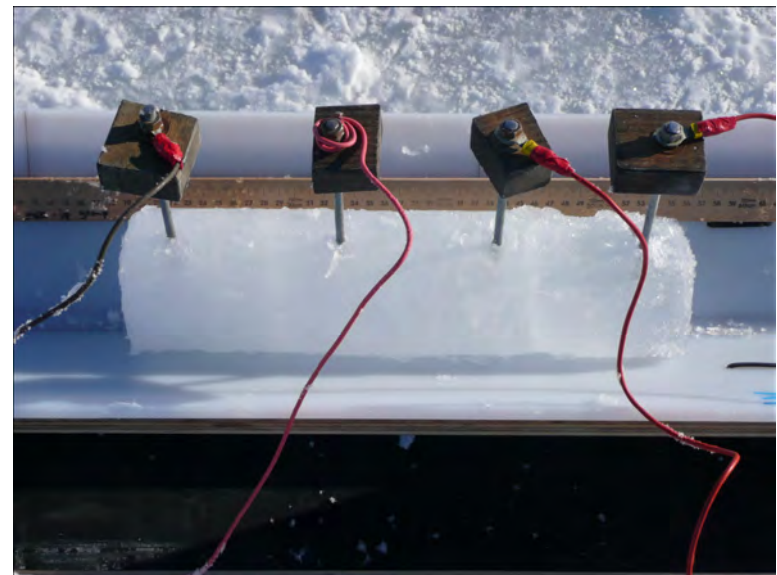
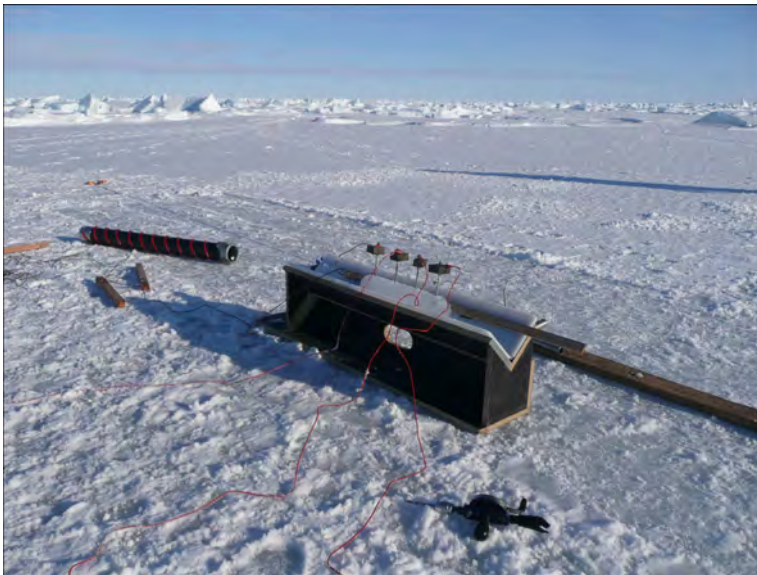
***measuring
fluid permeability
of Antarctic sea ice***

SIPEX 2007

electrical measurements



Wenner array



vertical conductivity

Zhu, Golden, Gully, Sampson *Physica B* 2010

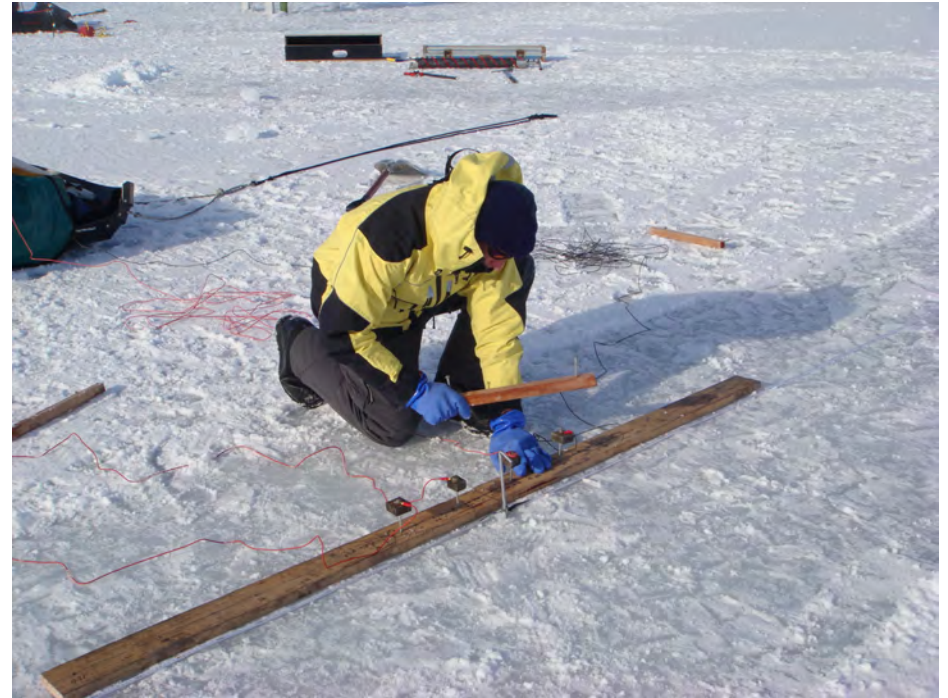
Sampson, Golden, Gully, Worby *Deep Sea Research* 2011

cross borehole tomography



***Ingham, Jones, Buchanan
Victoria University, Wellington, NZ***

Measuring sea ice thickness





Remote sensing of sea ice



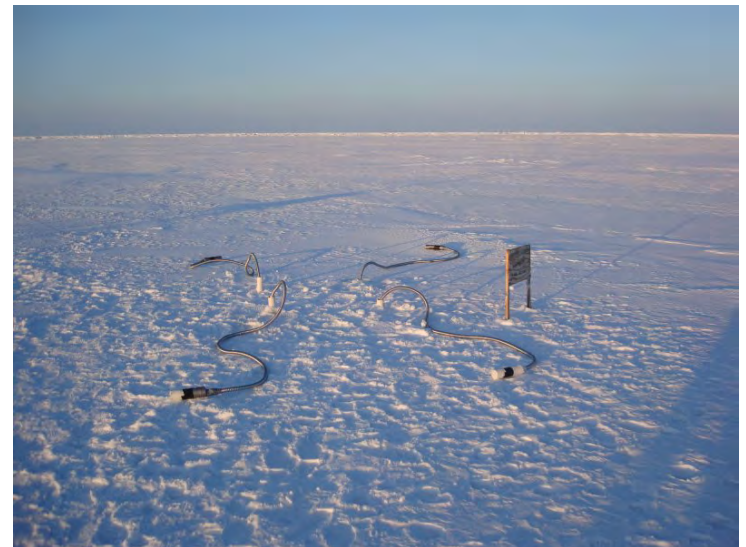
sea ice thickness
ice concentration

INVERSE PROBLEM

Recover sea ice
properties from
electromagnetic
(EM) data

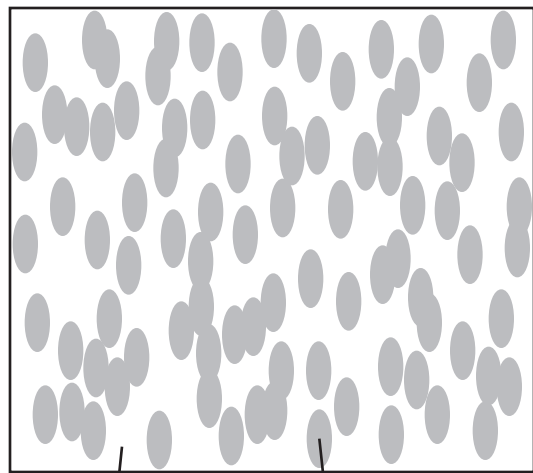
$$\epsilon^*$$

effective complex permittivity
(dielectric constant, conductivity)



brine volume fraction
brine inclusion connectivity

Effective complex permittivity of a two phase composite in the quasistatic (long wavelength) limit



ϵ_1

ϵ_2



ϵ^*

$$D = \epsilon E$$

$$\nabla \cdot D = 0$$

$$\nabla \times E = 0$$

$$\langle D \rangle = \epsilon^* \langle E \rangle$$

p_1, p_2 = volume fractions of
the components

$$\epsilon^* = \epsilon^* \left(\frac{\epsilon_1}{\epsilon_2}, \text{ composite geometry} \right)$$

**What are the effective propagation characteristics
of an EM wave (radar, microwaves) in the medium?**

Analytic Continuation Method for Homogenization

Bergman (1978), Milton (1979), Golden and Papanicolaou (1983), Theory of Composites, Milton (2002)

Stieltjes integral representation for homogenized parameter

separates geometry from parameters

$$F(s) = 1 - \frac{\epsilon^*}{\epsilon_2} = \int_0^1 \frac{d\mu(z)}{s - z}$$

← geometry

← material parameters

$$s = \frac{1}{1 - \epsilon_1 / \epsilon_2}$$

μ

- spectral measure of self adjoint operator $\Gamma\chi$
- mass = p_1
- higher moments depend on n -point correlations

$$\Gamma = \nabla(-\Delta)^{-1}\nabla.$$

χ = characteristic function of the brine phase

$$E = s (s + \Gamma\chi)^{-1} e_k$$

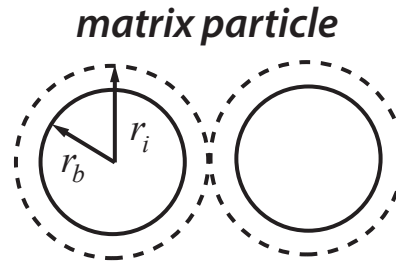
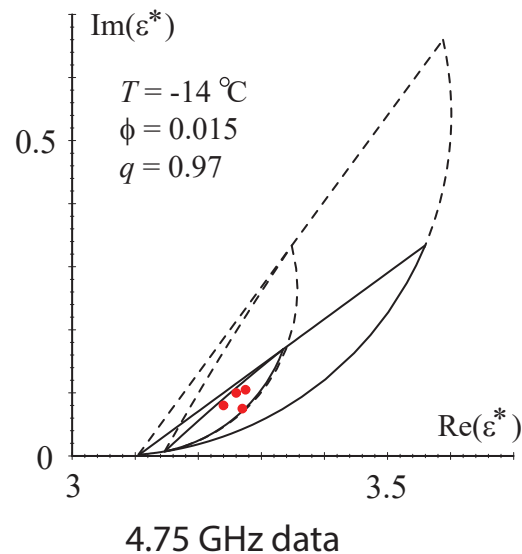
$\Gamma\chi$: microscale \rightarrow macroscale

$\Gamma\chi$ *links scales*

This representation distills the complexities of mixture geometry into the spectral properties of an operator like the Hamiltonian in physics.

forward and inverse bounds on the complex permittivity of sea ice

forward bounds

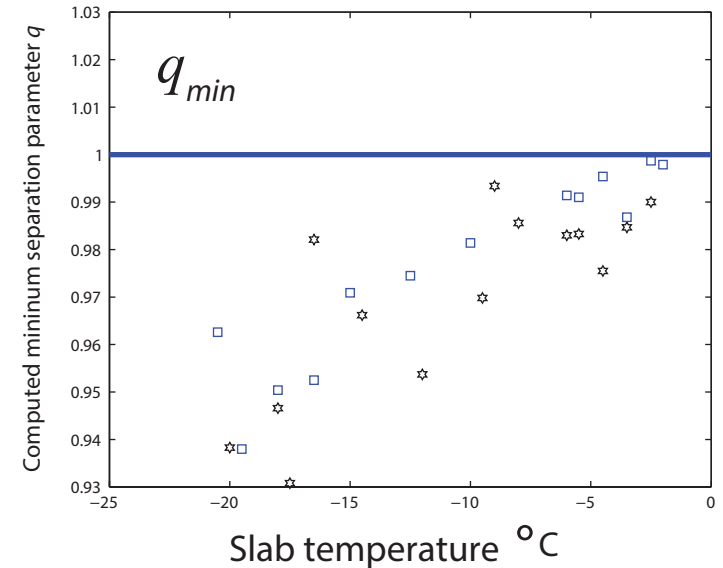


$$q = r_b / r_i$$

$$0 < q < 1$$

Golden 1995, 1997

inverse bounds



Inverse Homogenization

Cherkaev and Golden (1998), Day and Thorpe (1999), Cherkaev (2001), McPhedran, McKenzie, Milton (1982), *Theory of Composites*, Milton (2002)

ϵ^* \longrightarrow composite geometry
(spectral measure μ)

inverse bounds and recovery of brine porosity

Gully, Backstrom, Eicken, Golden
Physica B, 2007

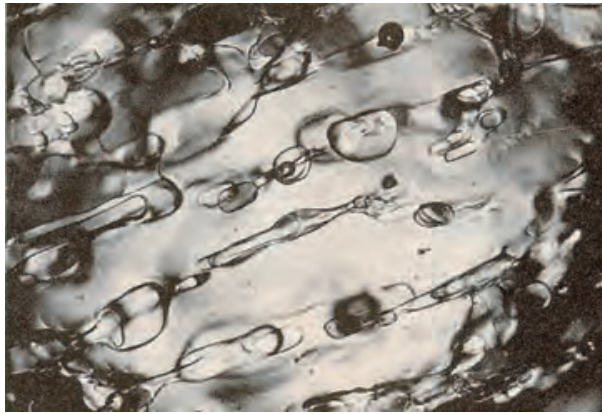
inversion for brine inclusion separations in sea ice from measurements of effective complex permittivity ϵ^*

rigorous inverse bound on spectral gap

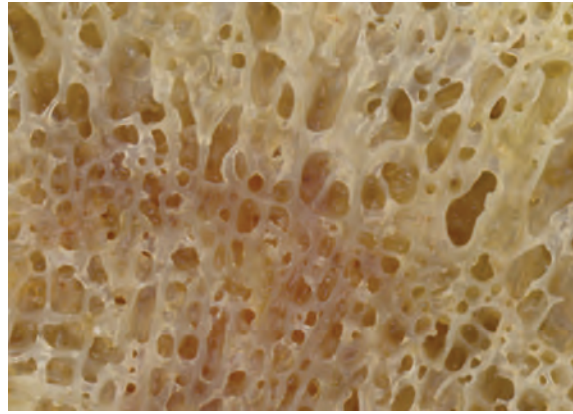
construct algebraic curves which bound admissible region in (p, q) -space

Orum, Cherkaev, Golden
Proc. Roy. Soc. A, 2012

SEA ICE

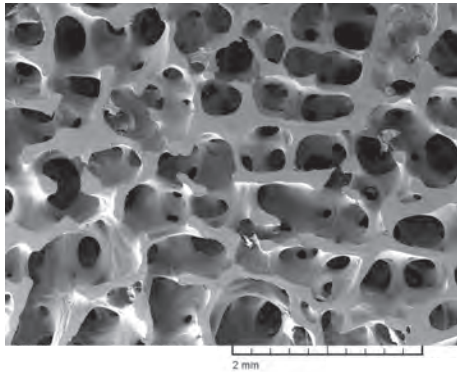


HUMAN BONE

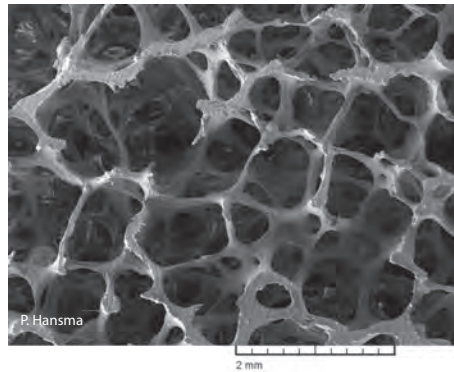


*spectral characterization
of porous microstructures
in human bone*

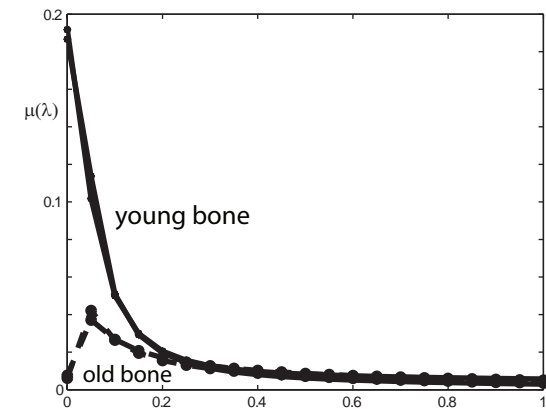
young healthy trabecular bone



old osteoporotic trabecular bone



reconstruct spectral measures
from complex permittivity data



use regularized inversion scheme

*apply spectral measure analysis of brine connectivity and
spectral inversion to electromagnetic monitoring of osteoporosis*

Golden, Murphy, Cherkaev, J. Biomechanics 2011

the math doesn't care if it's sea ice or bone!

direct calculation of spectral measures

Murphy, Hohenegger, Cherkaev, Golden, *Comm. Math. Sci.* 2015

- depends only on the composite geometry
- discretization of microstructural image gives binary network
- fundamental operator becomes a random matrix
- spectral measure computed from eigenvalues and eigenvectors

**once we have the spectral measure μ it can be used in
Stieltjes integrals for other transport coefficients:**

***electrical and thermal conductivity, complex permittivity,
magnetic permeability, diffusion, fluid flow properties***

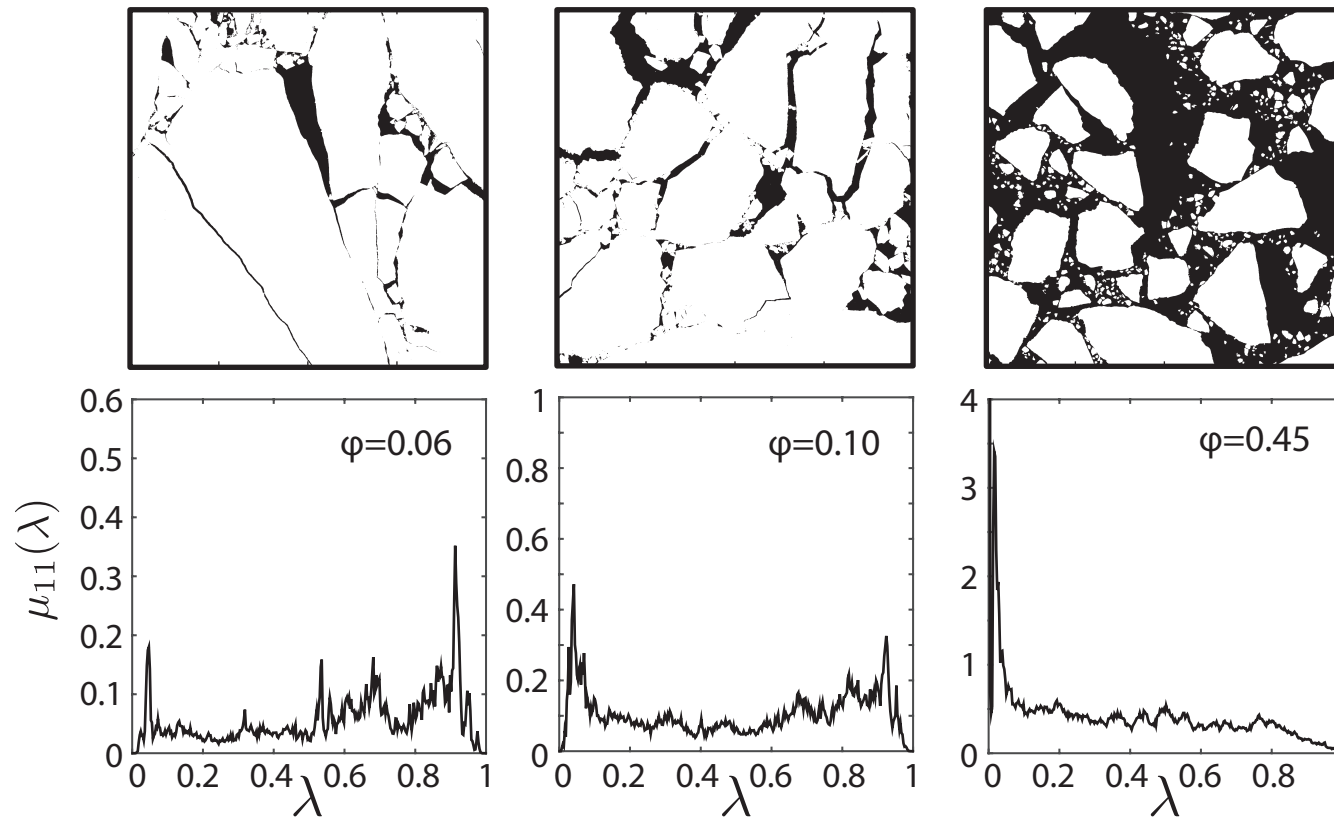
earlier studies of spectral measures

Day and Thorpe 1996

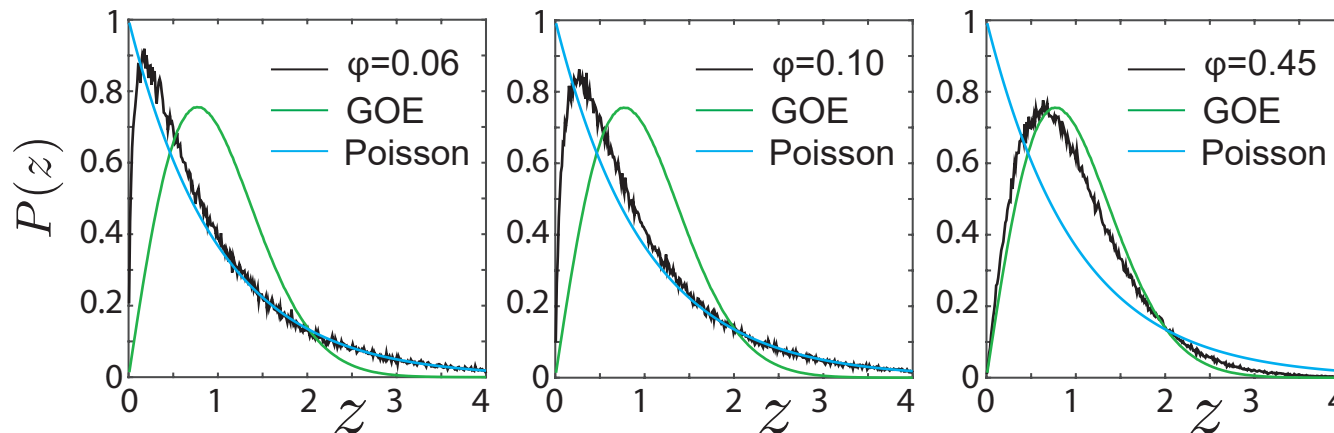
Helsing, McPhedran, Milton 2011

Spectral computations for sea ice floe configurations

spectral
measures



eigenvalue
spacing
distributions



uncorrelated



level repulsion

UNIVERSAL
Wigner-Dyson
distribution

Eigenvalue Statistics of Random Matrix Theory

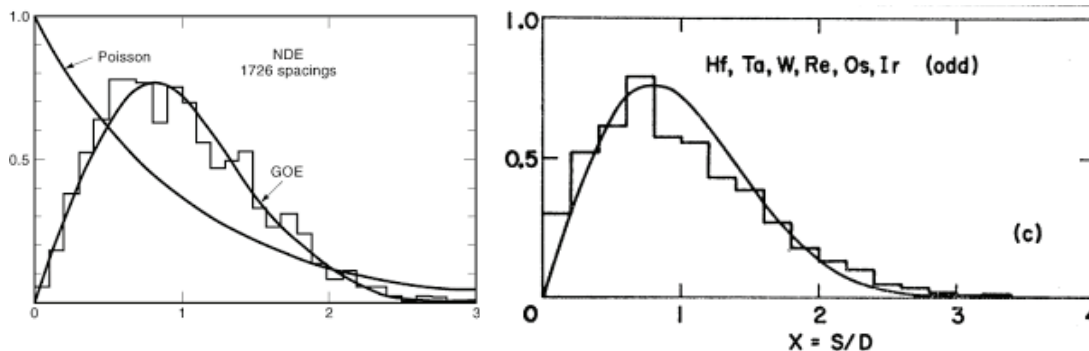
Wigner (1951) and Dyson (1953) first used random matrix theory (RMT) to describe quantized energy levels of heavy atomic nuclei.

$[N]_{ij} \sim N(0,1), \quad A = (N + N^T)/2 \quad \text{Gaussian orthogonal ensemble (GOE)}$

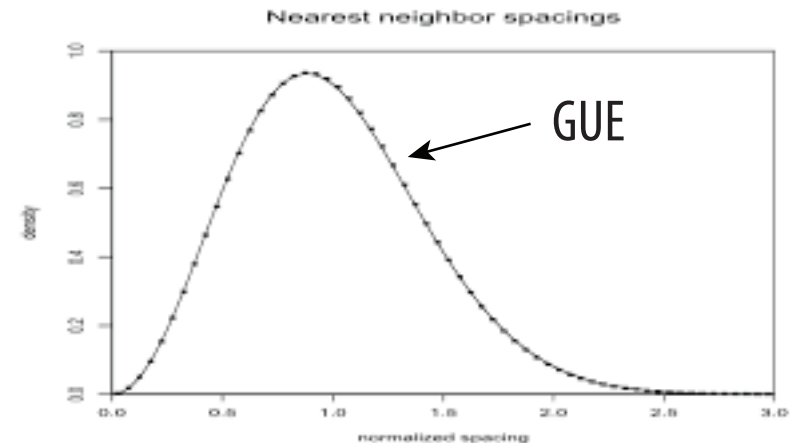
$[N]_{ij} \sim N(0,1) + iN(0,1), \quad A = (N + N^\dagger)/2 \quad \text{Gaussian unitary ensemble (GUE)}$

Short range and long range correlations of eigenvalues are measured by various eigenvalue statistics.

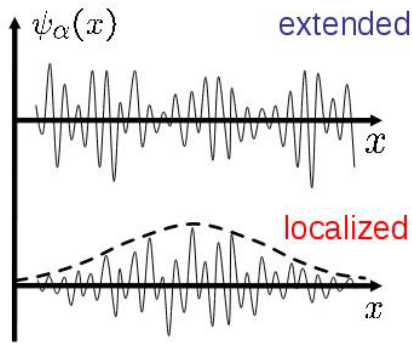
Spacing distributions of energy levels for heavy atomic nuclei



Spacing distributions of the first billion zeros of the Riemann zeta function



Universal eigenvalue statistics arise in a broad range of “unrelated” problems!



electronic transport in semiconductors

metal / insulator transition

localization

Anderson 1958
Mott 1949
Shklovshii et al 1993
Evangelou 1992

**Anderson transition in wave physics:
 quantum, optics, acoustics, water waves, ...**

from analysis of spectral measures for brine, melt ponds, ice floes

we find percolation-driven

Anderson transition for classical transport in composites

Murphy, Cherkaev, Golden Phys. Rev. Lett. 2017

**PERCOLATION
 TRANSITION**



**universal eigenvalue statistics (GOE)
 extended states, mobility edges**

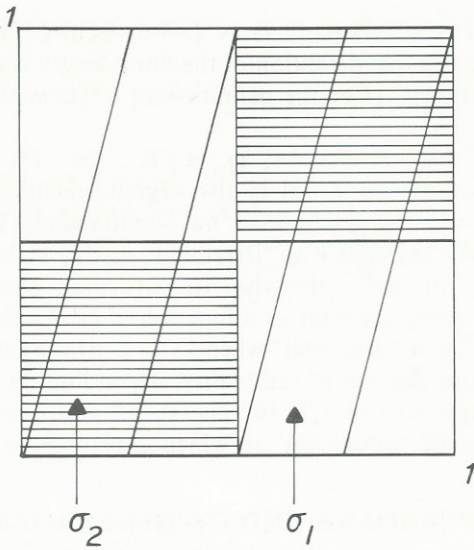
-- but with NO wave interference or scattering effects ! --

Classical transport in quasiperiodic media

Golden, Goldstein, and Lebowitz

Phys. Rev. Lett. 1985

J. Stat. Phys. 1990



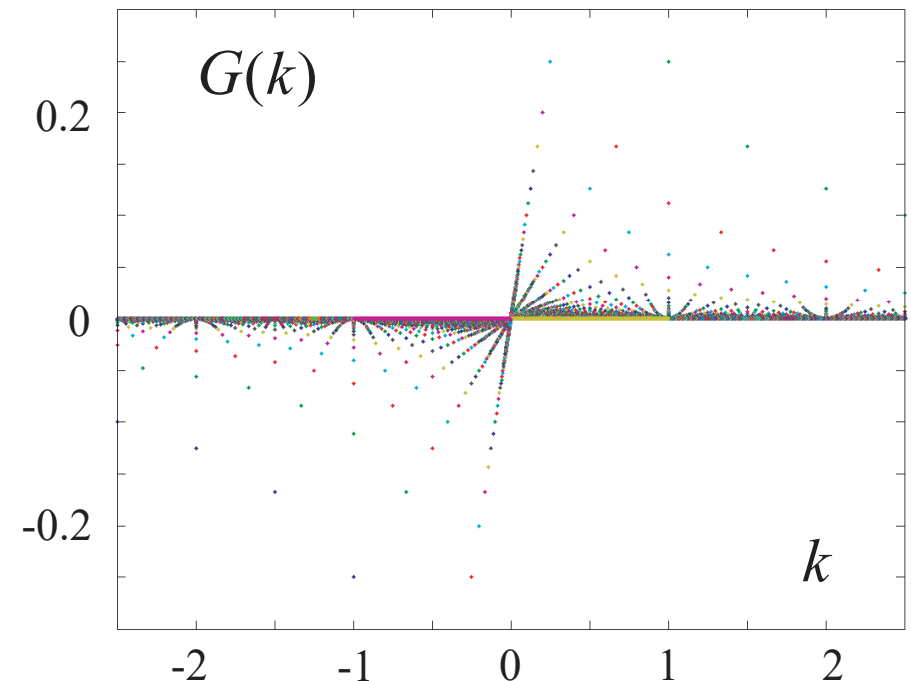
line of slope k through
an infinite checkerboard

effective conductivity $\sigma^*(k)$

effective resistivity $1/\sigma^*(k) = 1 - G(k)$

$$G(k) = \begin{cases} 0, & k \text{ irrational} \\ 1/pq, & k = p/q \text{ rational} \end{cases}$$

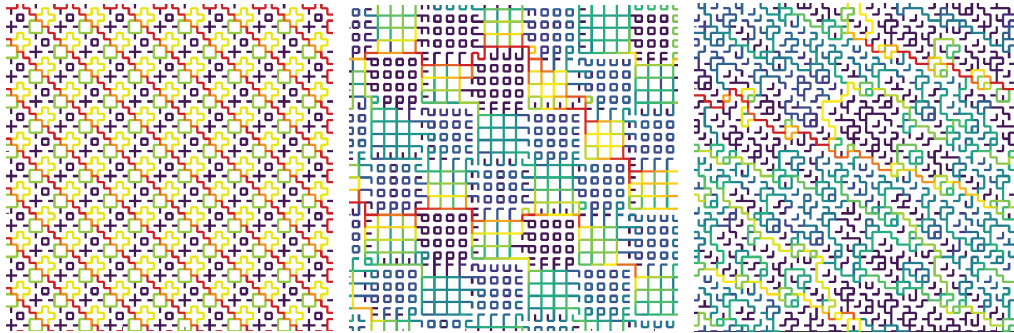
continuous at k irrational
discontinuous at k rational



Order to disorder in quasiperiodic composites

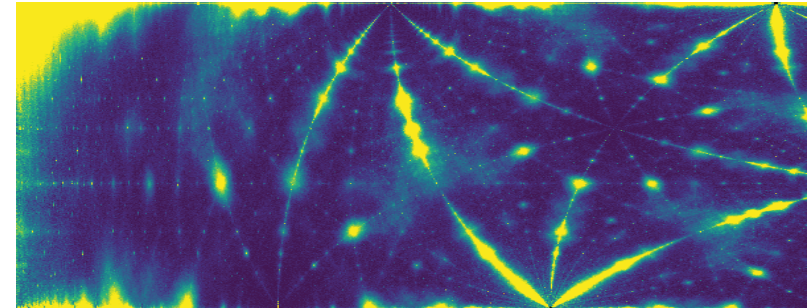
Morison, Murphy, Cherkaev, Golden, *Commun. Phys.* 2022

Parameterized Moiré Pattern Creates Tunable Microgeometry



Anderson transition as QP is tuned

Poisson
Wigner-Dyson



parameter space

periodic

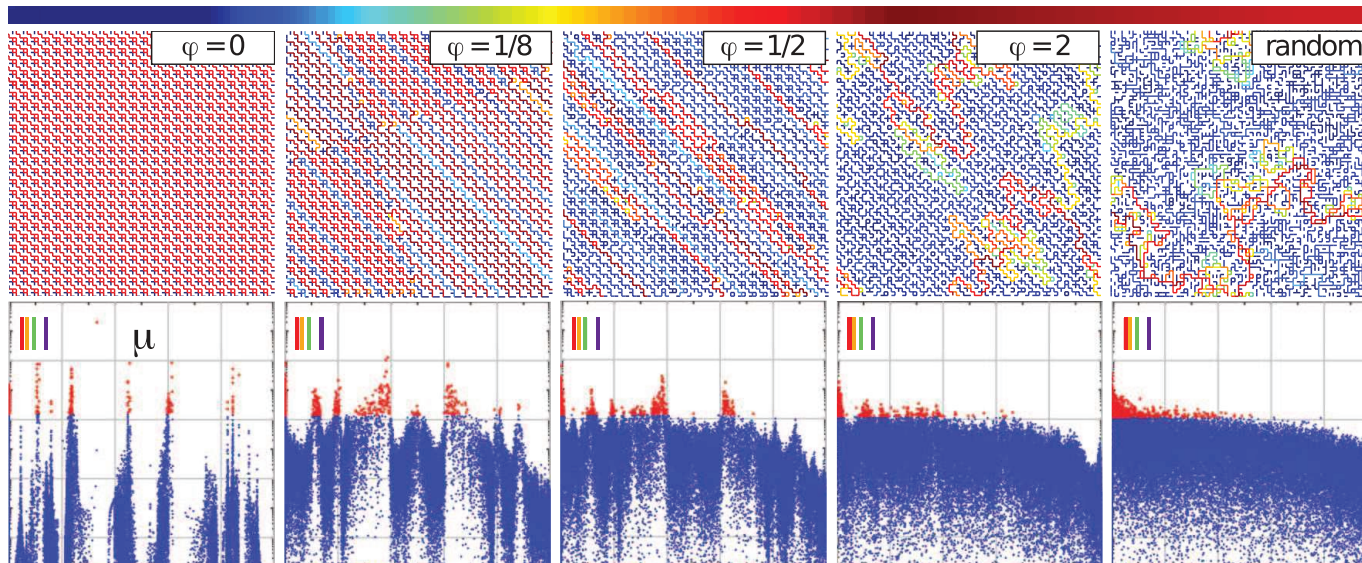


quasiperiodic

electric field
strength

spectral
measure

10^{-4}
 10^{-6}
 10^{-8}

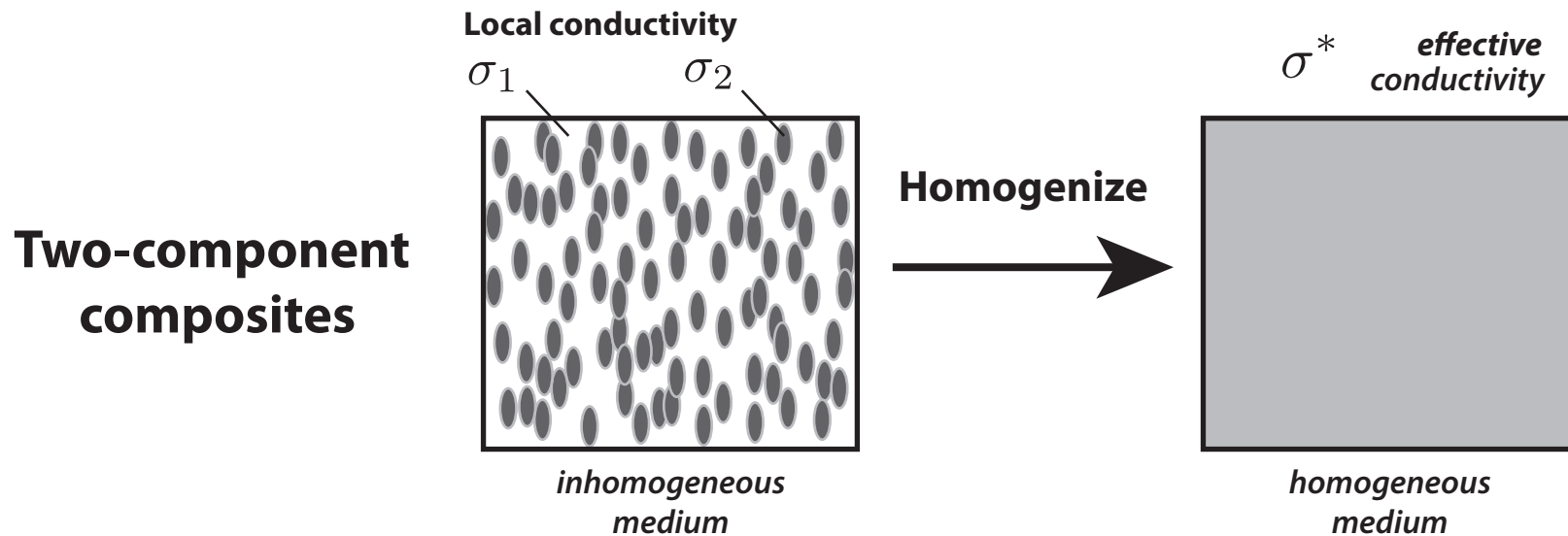


RRN at
percolation
threshold

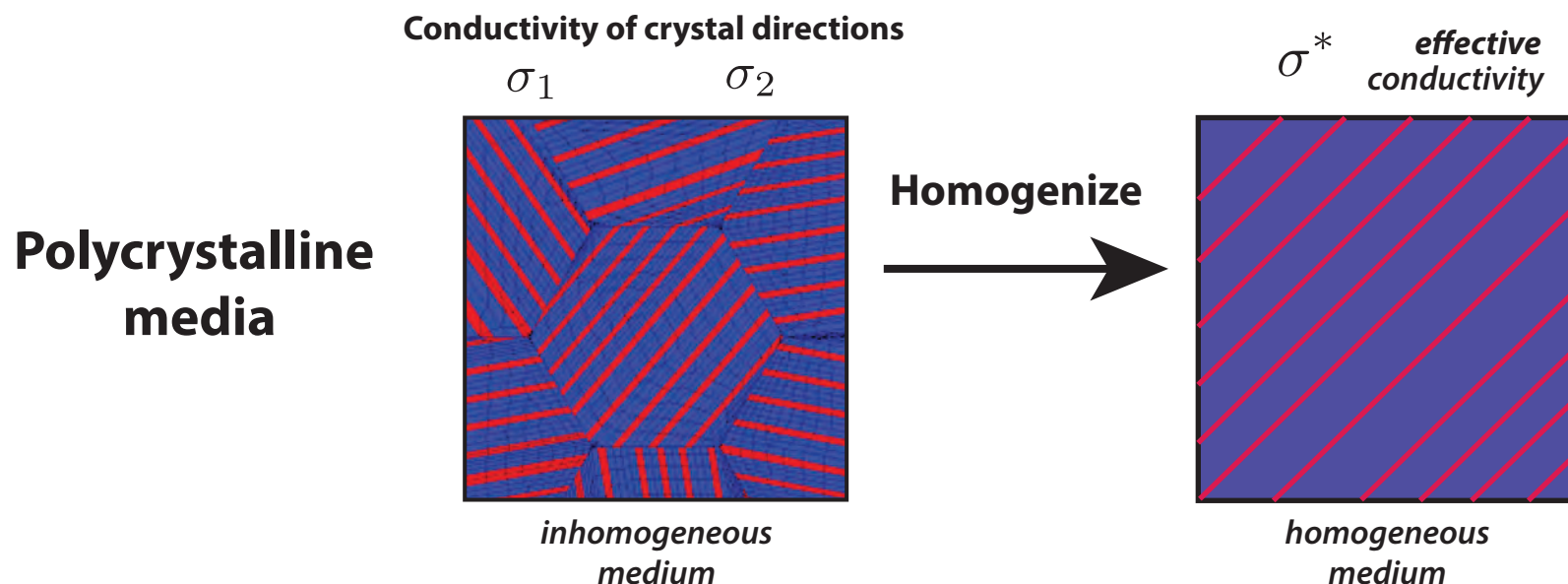
we bring the framework of solid state physics of electronic transport and band gaps in semiconductors to classical transport in periodic and quasiperiodic composites

photonic crystals and quasicrystals

Homogenization for polycrystalline materials



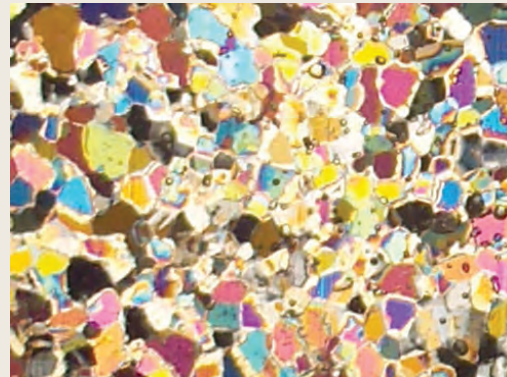
Find the homogeneous medium which behaves macroscopically the same as the inhomogeneous medium



Bounds on the complex permittivity of polycrystalline materials by analytic continuation

Adam Gully, Joyce Lin,
Elena Cherkaev, Ken Golden

- **Stieltjes integral representation for effective complex permittivity**
Milton (1981, 2002), Barabash and Stroud (1999), ...
- **Forward and inverse bounds**
orientation statistics
- **Applied to sea ice using two-scale homogenization**
- **Inverse bounds give method for distinguishing ice types using remote sensing techniques**



PROCEEDINGS A

350 YEARS
OF SCIENTIFIC
PUBLISHING

An invited review
commemorating 350 years
of scientific publishing at the
Royal Society

A method to distinguish
between different types
of sea ice using remote
sensing techniques

A computer model to
determine how a human
should walk so as to expend
the least energy



THE
ROYAL
SOCIETY
PUBLISHING

higher threshold for fluid flow in granular sea ice

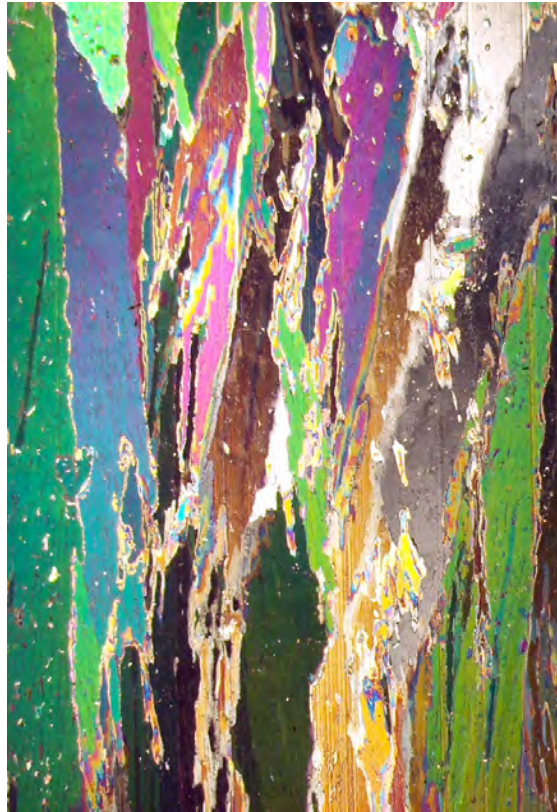
microscale details impact “mesoscale” processes

nutrient fluxes for microbes
melt pond drainage
snow-ice formation

columnar

granular

5%



10%



Golden, Sampson, Gully, Lubbers, Tison 2022

electromagnetically distinguishing ice types
Kitsel Lusted, Elena Cherkaev, Ken Golden

mesoscale

wave propagation in the marginal ice zone (MIZ)

Stieltjes integral representation and bounds for the complex viscoelasticity of the ice - ocean layer

Sampson, Murphy, Cherkaev, Golden 2022

first theory of key parameter in wave-ice interactions only fitted to wave data before

Keller, 1998

Mosig, Montiel, Squire, 2015

Wang, Shen, 2012

Analytic Continuation Method

Bergman (78) - Milton (79)
integral representation for ϵ^*

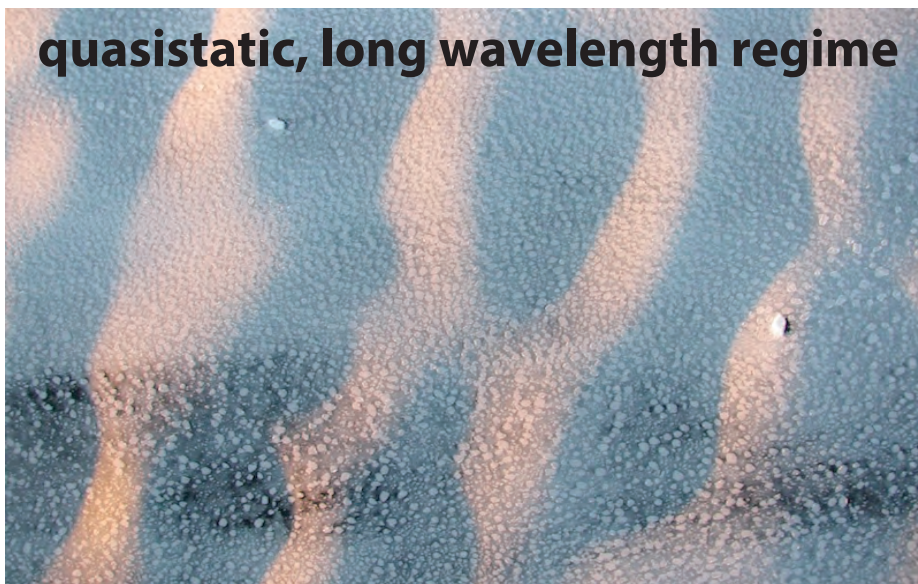
Golden and Papanicolaou (83)

Milton, *Theory of Composites* (02)

quasistatic, long wavelength regime

homogenized parameter depends on sea ice concentration and ice floe geometry

like EM waves



advection enhanced diffusion

effective diffusivity

nutrient and salt transport in sea ice
heat transport in sea ice with convection
sea ice floes in winds and ocean currents
tracers, buoys diffusing in ocean eddies
diffusion of pollutants in atmosphere

advection diffusion equation with a velocity field \vec{u}

$$\frac{\partial T}{\partial t} + \vec{u} \cdot \vec{\nabla} T = \kappa_0 \Delta T$$

$$\vec{\nabla} \cdot \vec{u} = 0$$



homogenize

$$\frac{\partial \bar{T}}{\partial t} = \kappa^* \Delta \bar{T}$$

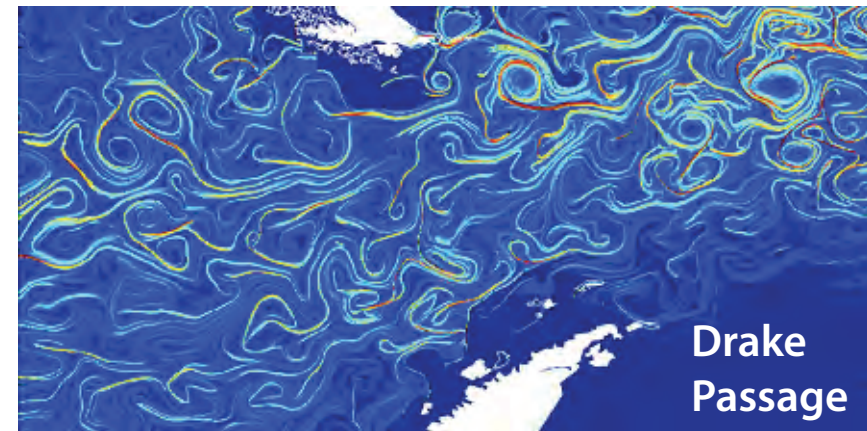
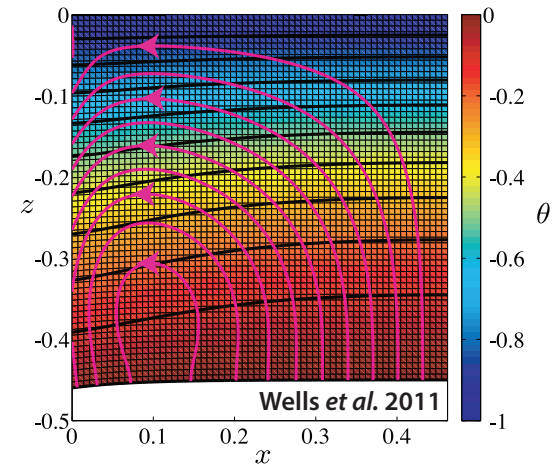
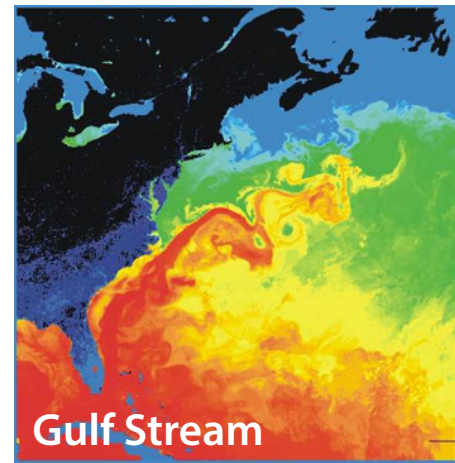
κ^* effective diffusivity

Stieltjes integral for κ^* with spectral measure

Avellaneda and Majda, PRL 89, CMP 91

Murphy, Cherkaev, Xin, Zhu, Golden, *Ann. Math. Sci. Appl.* 2017

Murphy, Cherkaev, Zhu, Xin, Golden, *J. Math. Phys.* 2020



tracers flowing through inverted sea ice blocks



Stieltjes Integral Representation for Advection Diffusion

Murphy, Cherkaev, Zhu, Xin, Golden, *J. Math. Phys.* 2020

$$\kappa^* = \kappa \left(1 + \int_{-\infty}^{\infty} \frac{d\mu(\tau)}{\kappa^2 + \tau^2} \right), \quad F(\kappa) = \int_{-\infty}^{\infty} \frac{d\mu(\tau)}{\kappa^2 + \tau^2}$$

- μ is a positive definite measure corresponding to the spectral resolution of the self-adjoint operator $i\Gamma H\Gamma$
- H = stream matrix , κ = local diffusivity
- $\Gamma := -\nabla(-\Delta)^{-1}\nabla$, Δ is the Laplace operator
- $i\Gamma H\Gamma$ is bounded for time independent flows
- $F(\kappa)$ is analytic off the spectral interval in the κ -plane

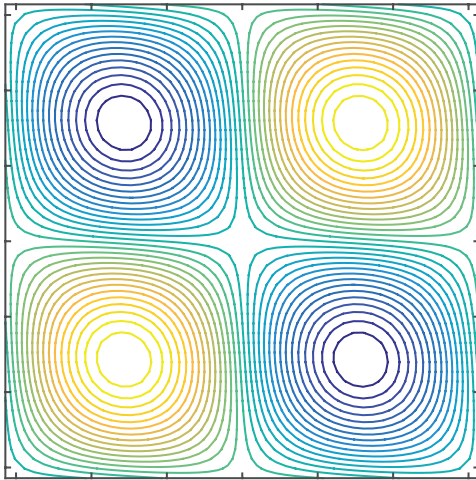
rigorous framework for numerical computations of spectral measures and effective diffusivity for model flows

new integral representations, theory of moment calculations

separation of material properties and flow field

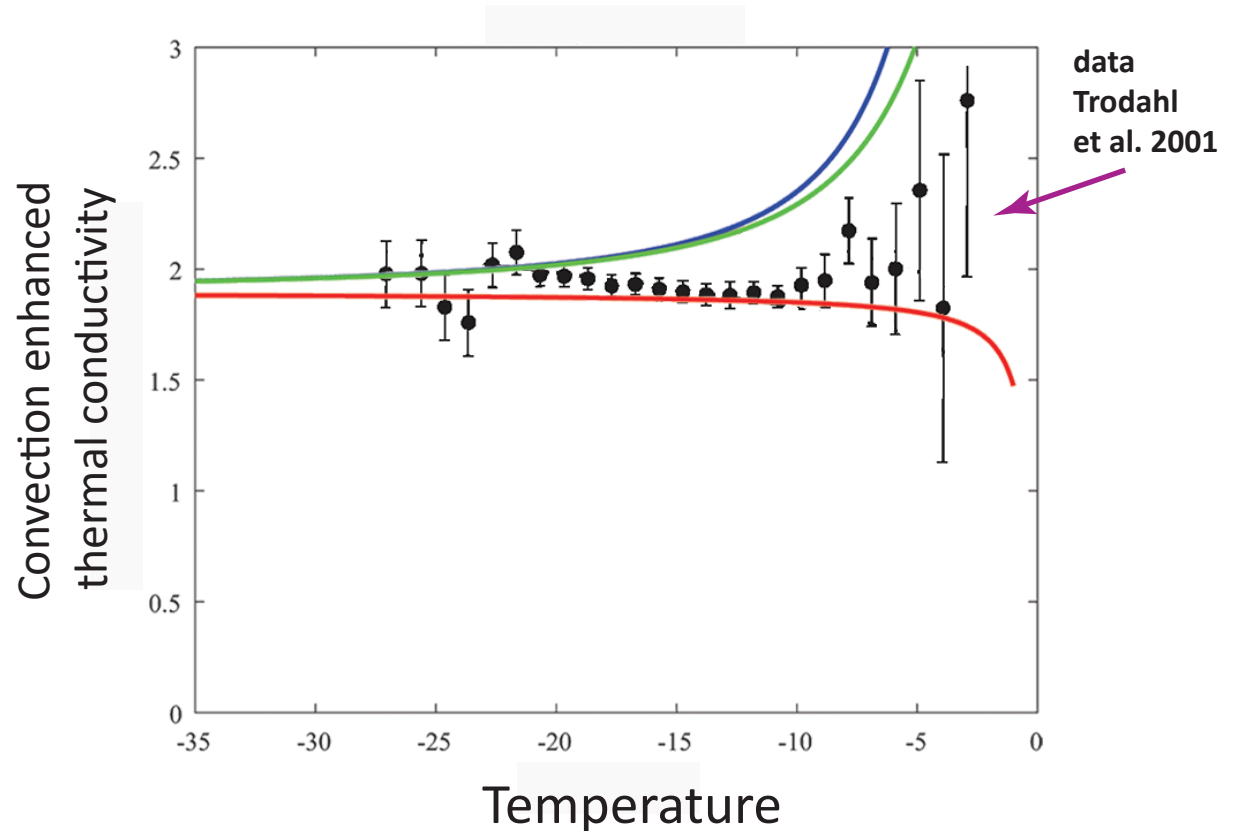
Rigorous bounds on convection enhanced thermal conductivity of sea ice

Kraitzman, Hardenbrook, Dinh, Murphy, Zhu, Cherkaev, Golden 2022



cat's eye flow model for
brine convection cells

similar bounds
for shear flows



rigorous Padé bounds from Stieltjes integral +
analytical calculations of moments of measure

melt pond formation and albedo evolution:

- *major drivers in polar climate*
- *key challenge for global climate models*

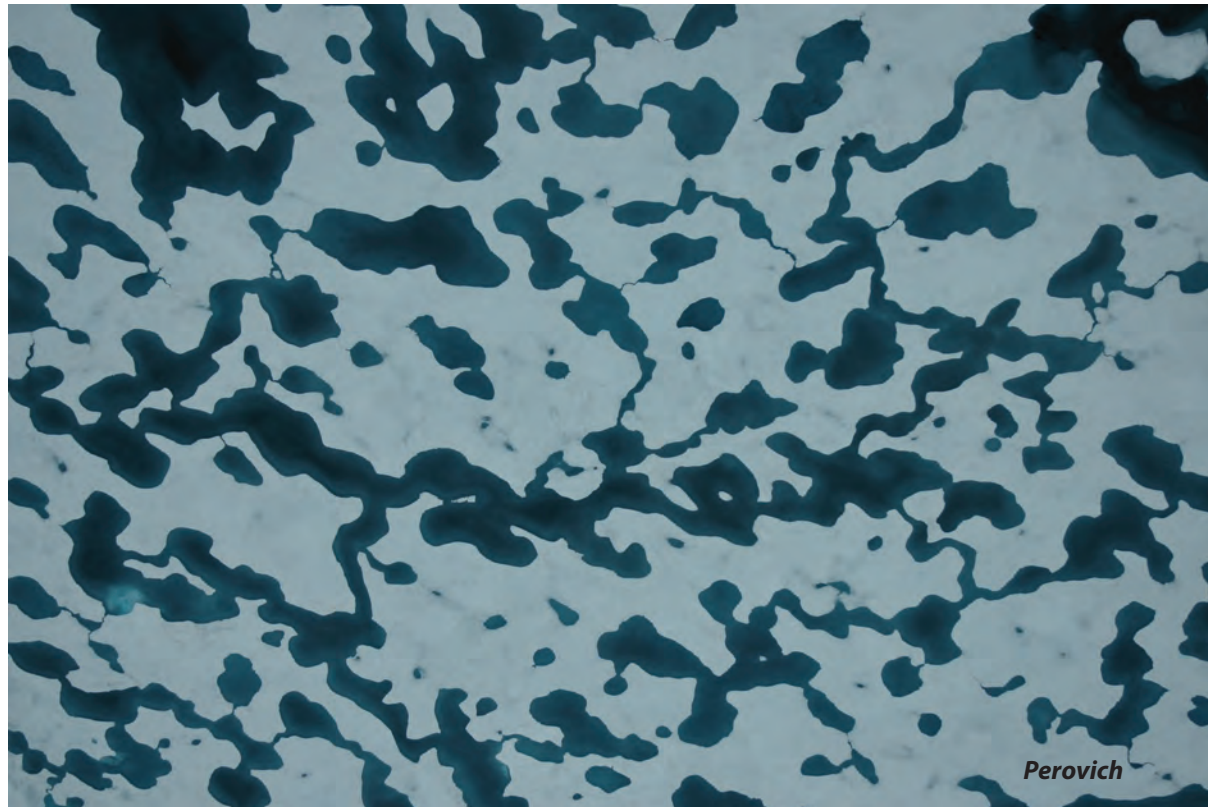
numerical models of melt pond evolution, including topography, drainage (permeability), etc.

Lüthje, Feltham,
Taylor, Worster 2006

Flocco, Feltham 2007

Skyllingstad, Paulson,
Perovich 2009

Flocco, Feltham,
Hunke 2012



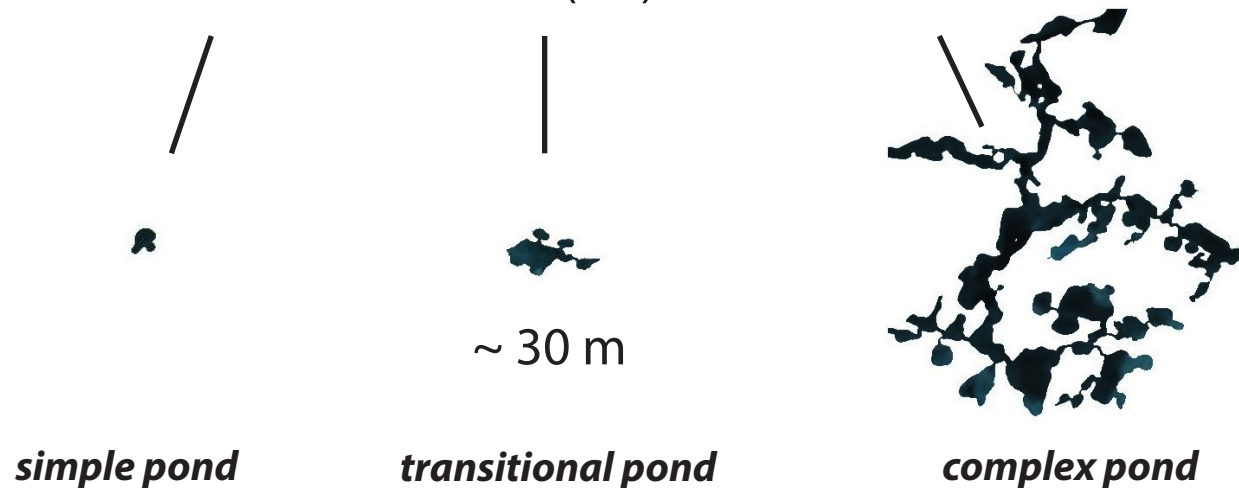
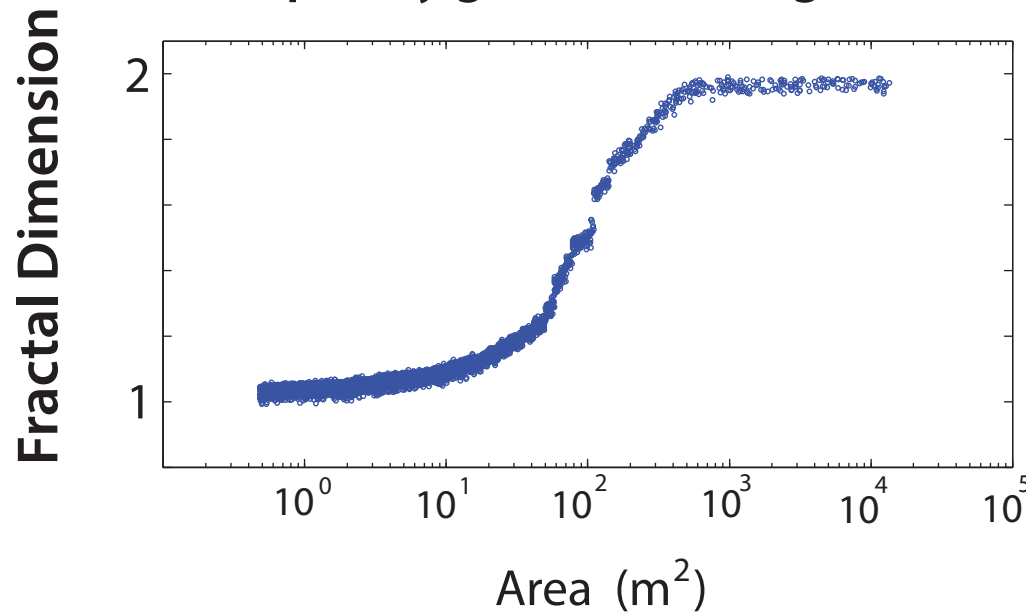
Are there universal features of the evolution similar to phase transitions in statistical physics?

Transition in the fractal geometry of Arctic melt ponds

Christel Hohenegger, Bacim Alali, Kyle Steffen, Don Perovich, Ken Golden

The Cryosphere, 2012

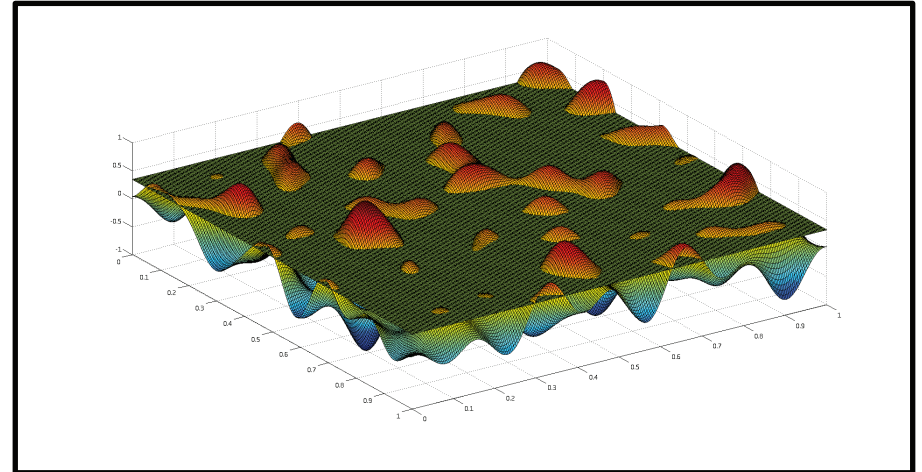
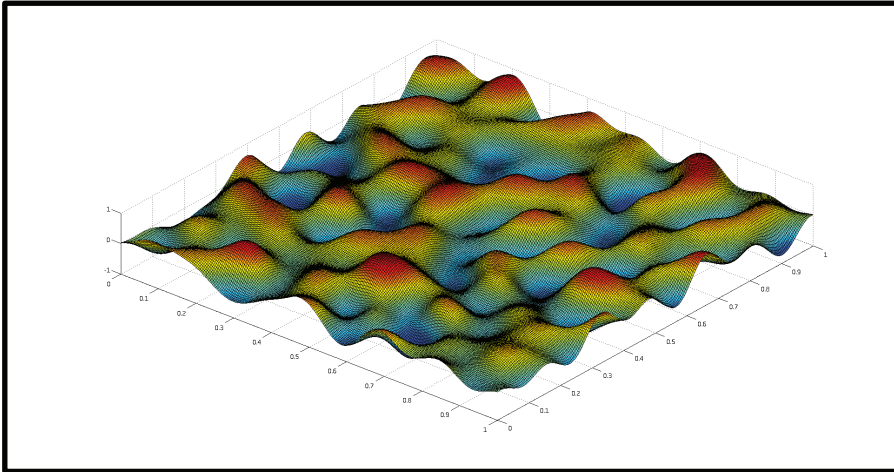
complexity grows with length scale



Continuum percolation model for melt pond evolution

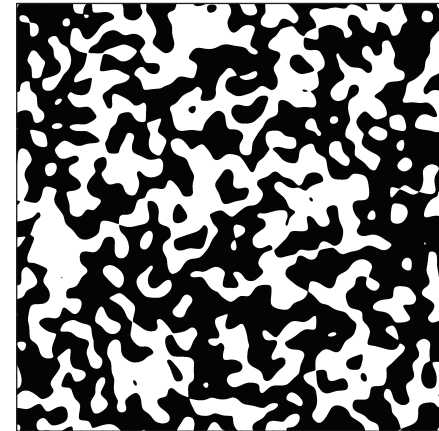
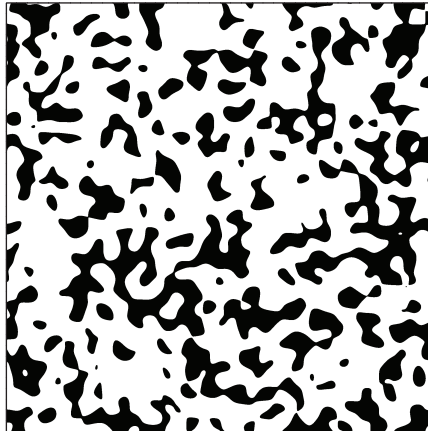
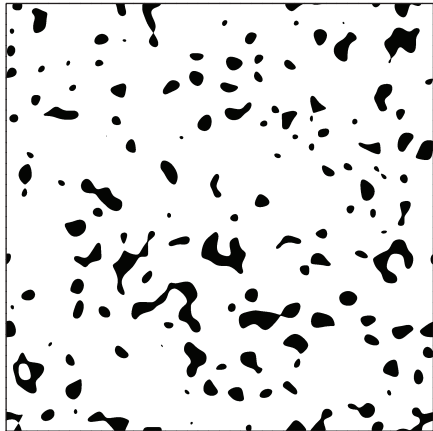
level sets of random surfaces

Brady Bowen, Court Strong, Ken Golden, J. Fractal Geometry 2018



random Fourier series representation of surface topography

intersections of a plane with the surface define melt ponds

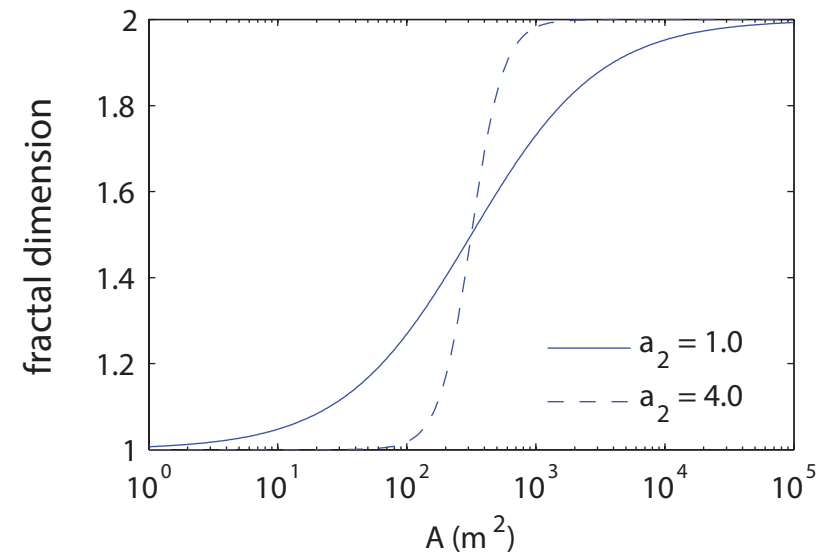
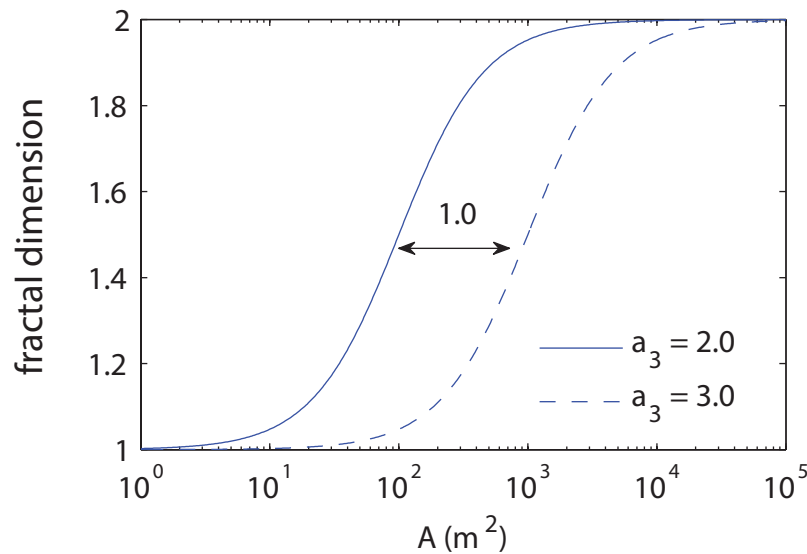


electronic transport in disordered media

diffusion in turbulent plasmas

Isichenko, Rev. Mod. Phys., 1992

fractal dimension curves depend on statistical parameters defining random surface



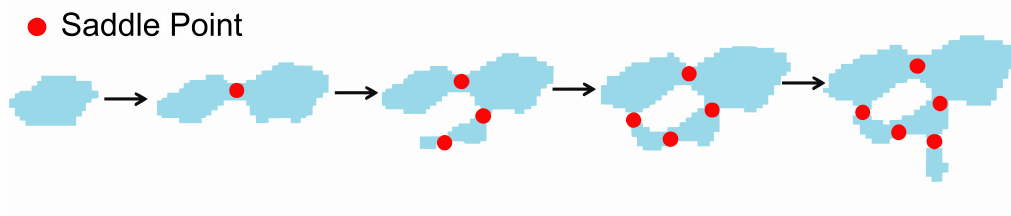
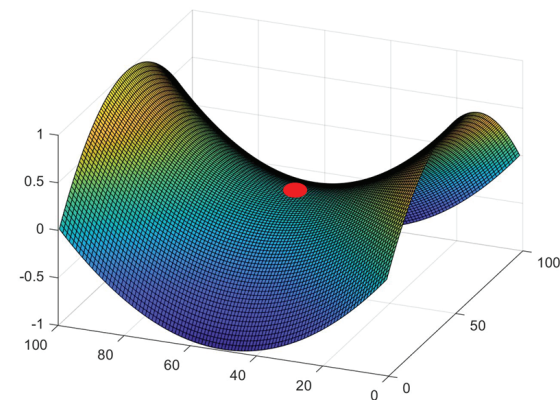
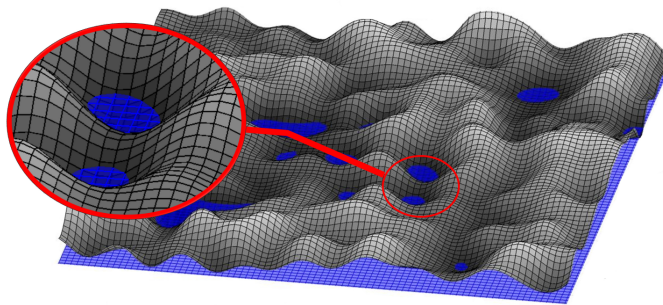
Saddle points of the sea ice surface and the fractal geometry of Arctic melt ponds

Physical Review Research (invited, under review)

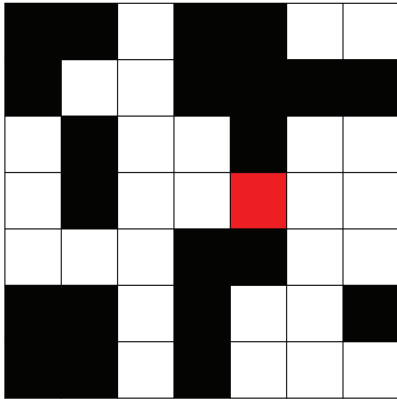
Ryleigh Moore, Jacob Jones, Dane Gollero,
Court Strong, Ken Golden

Several models replicate the transition in fractal dimension, but none explain how it arises.

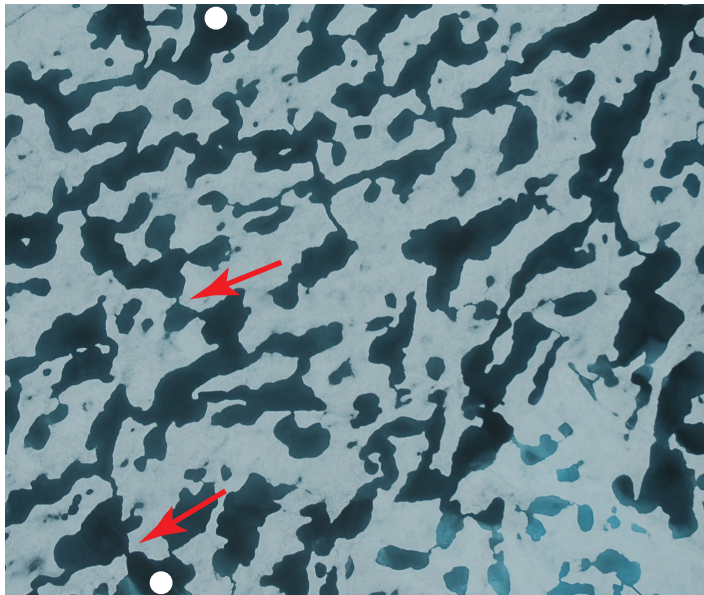
We use Morse theory applied to the random surface model to show that **saddle points** play the critical role in the fractal transition.



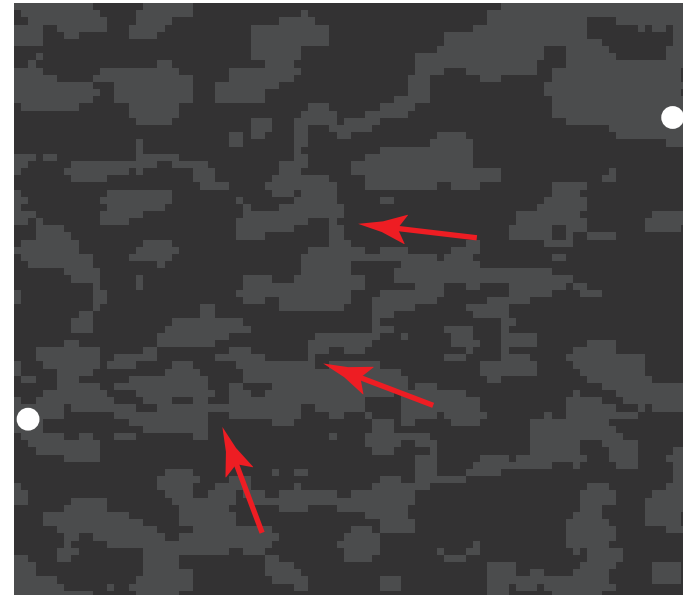
ponds coalesce
(change topology) and
complexify at saddle points



- Ponds connect through saddle points (Morse Theory).
- Red bonds in lattice percolation theory ~ saddle points.



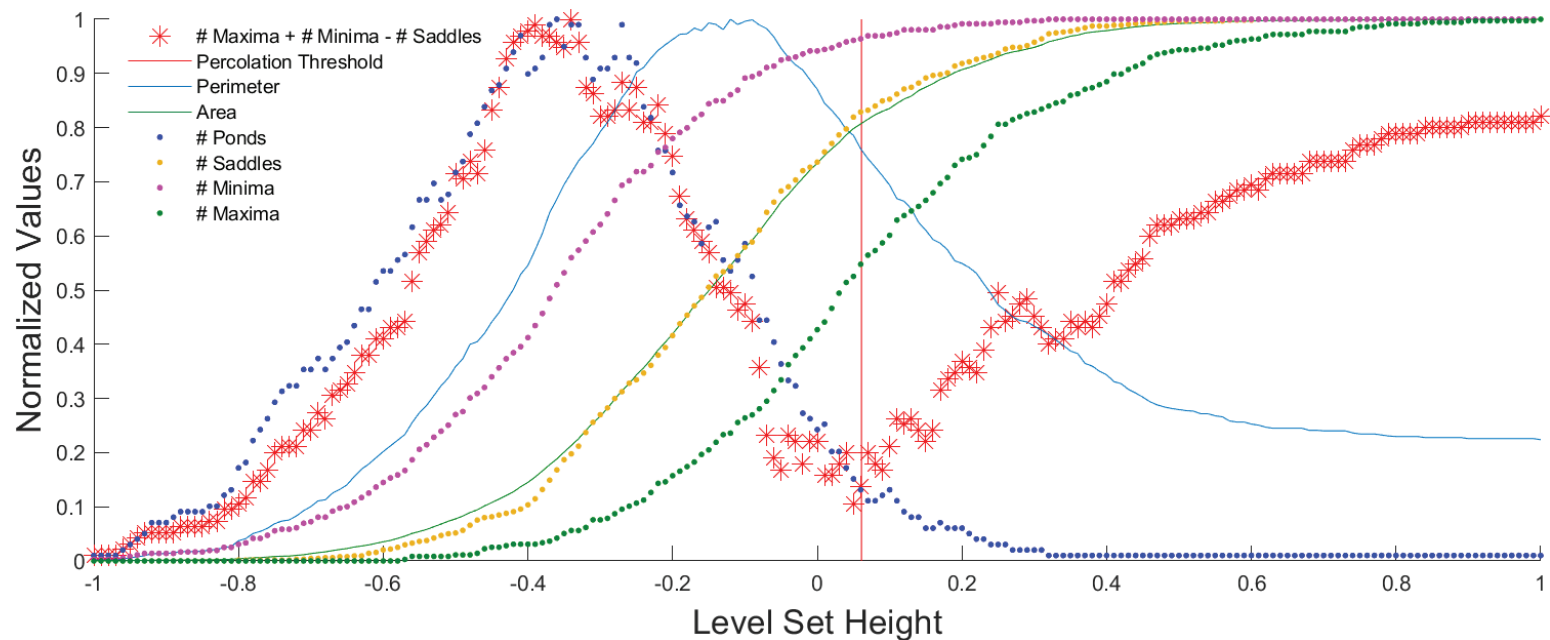
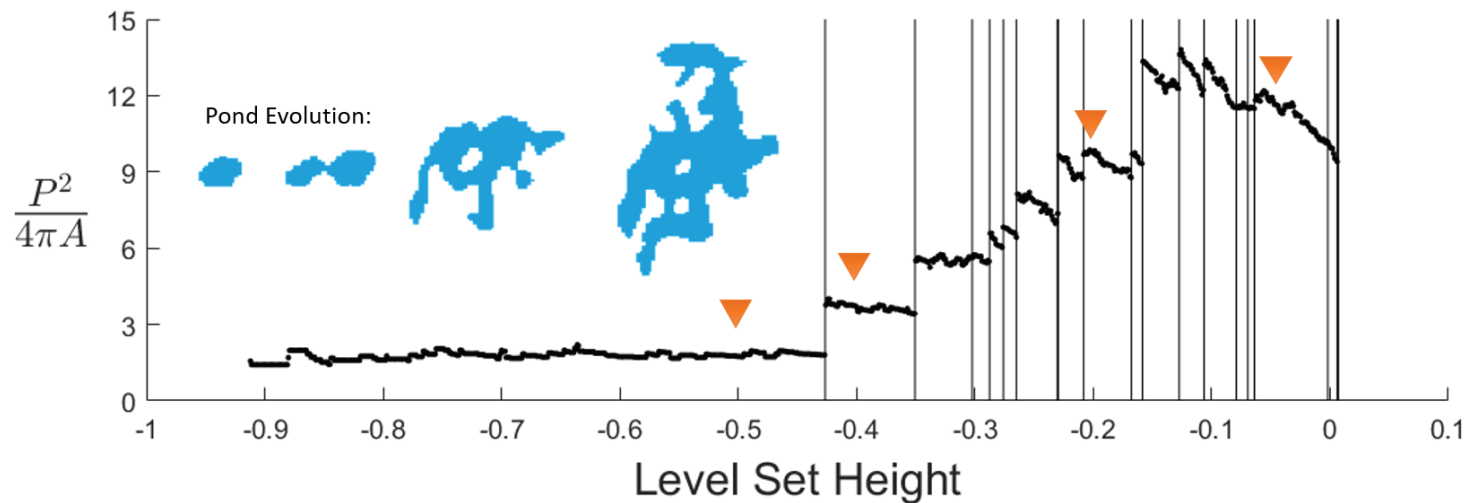
saddles



"red squares"

Main results

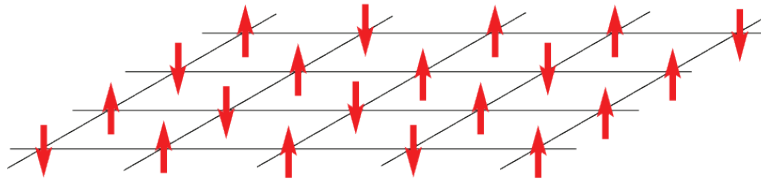
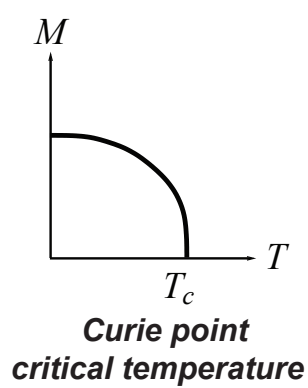
Isoperimetric quotient - as a proxy for fractal dimension - takes discrete jumps up when ponds coalesce at saddle points.



Euler characteristic reaches minimum at percolation threshold.

Horizontal fluid permeability “controlled” by saddles ~ electronic transport in 2D random potential.

Ising Model for a Ferromagnet



applied
magnetic
field



$$s_i = \begin{cases} +1 & \text{spin up} \\ -1 & \text{spin down} \end{cases} \quad \begin{array}{l} \text{blue} \\ \text{white} \end{array}$$

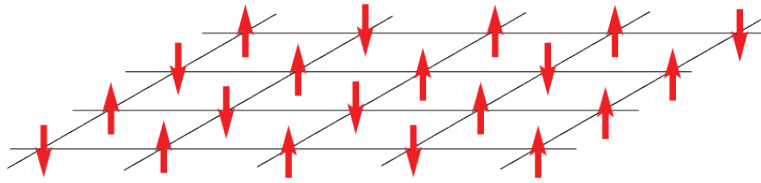
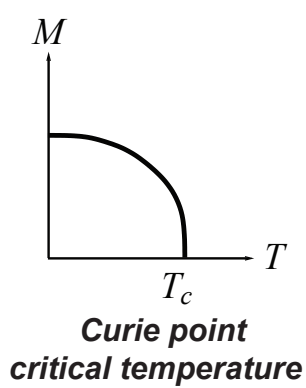
$$\mathcal{H} = -H \sum_i s_i - J \sum_{\langle i,j \rangle} s_i s_j$$

nearest neighbor Ising Hamiltonian

$$M(T, H) = \lim_{N \rightarrow \infty} \frac{1}{N} \left\langle \sum_j s_j \right\rangle$$

effective magnetization

Ising Model for a Ferromagnet



$$s_i = \begin{cases} +1 & \text{spin up} \\ -1 & \text{spin down} \end{cases} \quad \begin{matrix} \text{blue} \\ \text{white} \end{matrix}$$

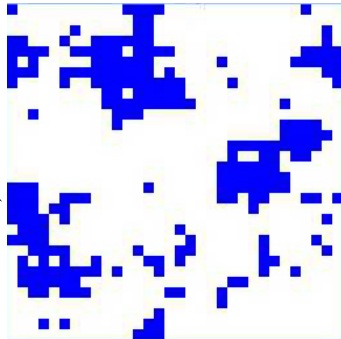
$$\mathcal{H} = -H \sum_i s_i - J \sum_{\langle i,j \rangle} s_i s_j$$

nearest neighbor Ising Hamiltonian

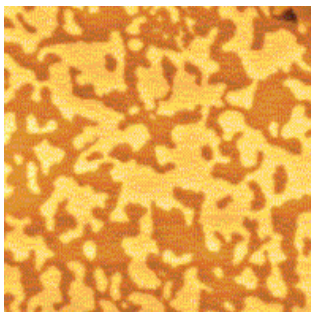
$$M(T, H) = \lim_{N \rightarrow \infty} \frac{1}{N} \left\langle \sum_j s_j \right\rangle$$

effective magnetization

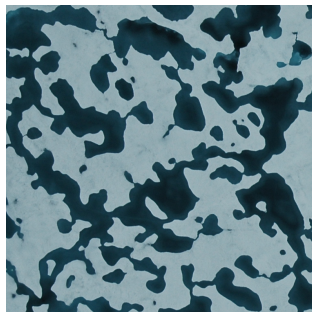
islands of like spins



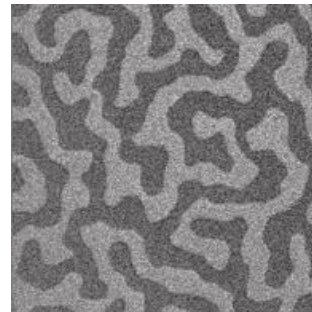
energy is lowered when nearby spins align with each other, forming **magnetic domains**



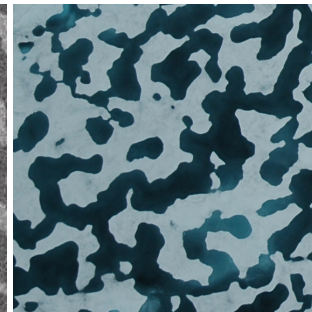
magnetic domains in cobalt



melt ponds (Perovich)



magnetic domains in cobalt-iron-boron



melt ponds (Perovich)

Ising model for ferromagnets \longrightarrow Ising model for melt ponds

Ma, Sudakov, Strong, Golden, *New J. Phys.*, 2019

$$\mathcal{H} = - \sum_i^N H_i s_i - J \sum_{\langle i,j \rangle}^N s_i s_j \quad s_i = \begin{cases} \uparrow & +1 \text{ water (spin up)} \\ \downarrow & -1 \text{ ice (spin down)} \end{cases}$$

random magnetic field
represents snow topography

magnetization M pond area fraction $F = \frac{(M+1)}{2}$ only nearest neighbor patches interact
 \sim albedo

Starting with random initial configurations, as Hamiltonian energy is minimized by Glauber spin flip dynamics, system “flows” toward metastable equilibria.

Order from Disorder

Ising model for ferromagnets \longrightarrow Ising model for melt ponds

Ma, Sudakov, Strong, Golden, *New J. Phys.*, 2019

$$\mathcal{H} = - \sum_i^N H_i s_i - J \sum_{\langle i,j \rangle}^N s_i s_j \quad s_i = \begin{cases} \uparrow & +1 \text{ water (spin up)} \\ \downarrow & -1 \text{ ice (spin down)} \end{cases}$$

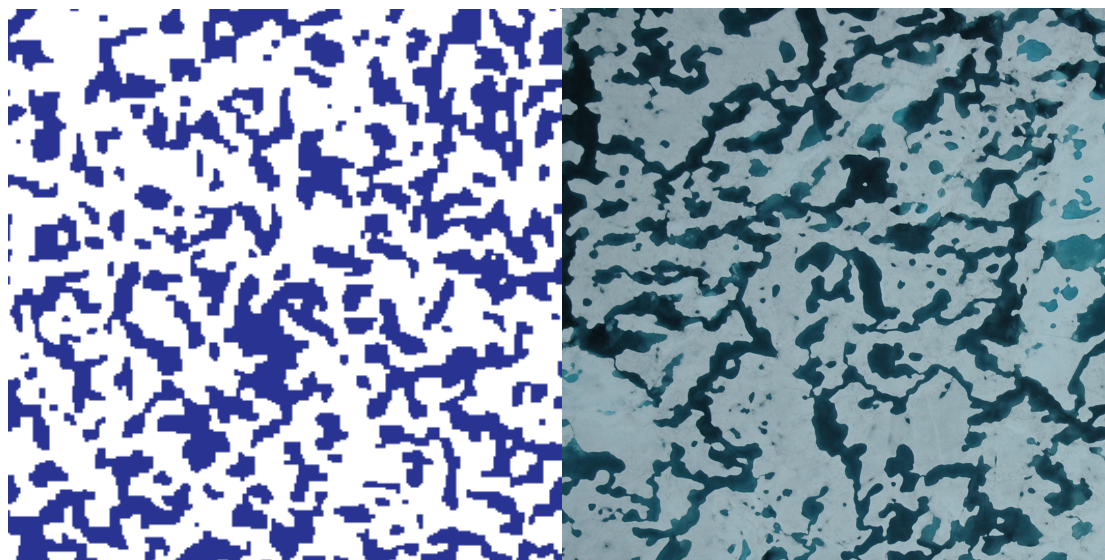
random magnetic field represents snow topography

magnetization M pond area fraction $F = \frac{(M+1)}{2}$ only nearest neighbor patches interact

$\sim \text{albedo}$

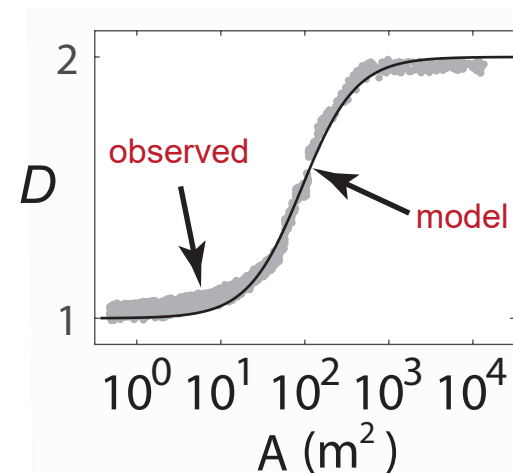
Starting with random initial configurations, as Hamiltonian energy is minimized by Glauber spin flip dynamics, system “flows” toward metastable equilibria.

Order from Disorder



Ising
model

melt pond
photo (Perovich)



pond size
distribution exponent

observed -1.5

(Perovich, et al. 2002)

model -1.58

Scientific American
EOS, PhysicsWorld, ...

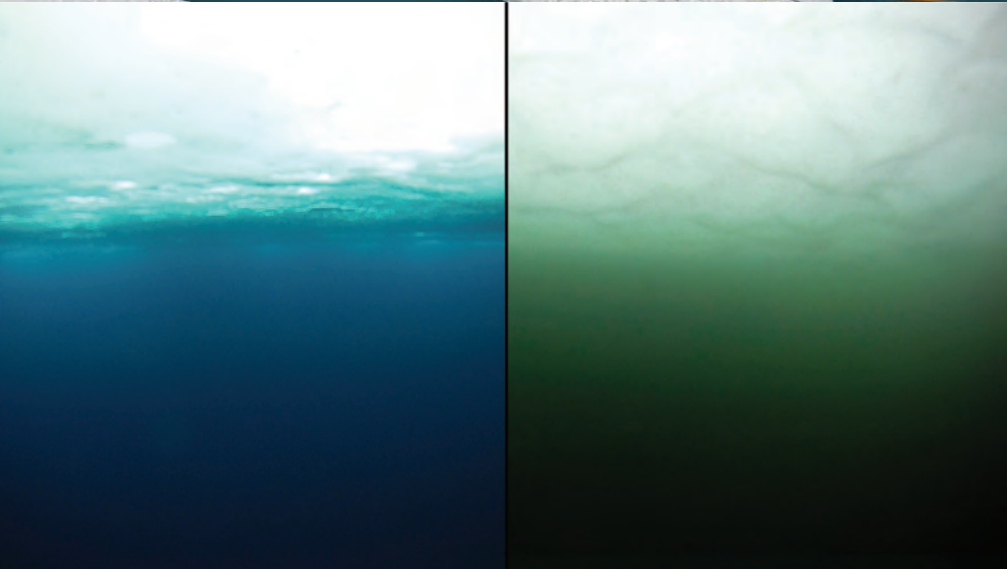
ONLY MEASURED INPUT = LENGTH SCALE (GRID SIZE) from snow topography data



Perovich

Melt ponds control transmittance of solar energy through sea ice, impacting upper ocean ecology.

WINDOWS



no bloom

bloom

massive under-ice **algal bloom**

Arrigo et al., *Science* 2012

Have we crossed into a new ecological regime?

The frequency and extent of sub-ice phytoplankton blooms in the Arctic Ocean

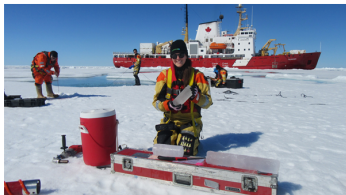
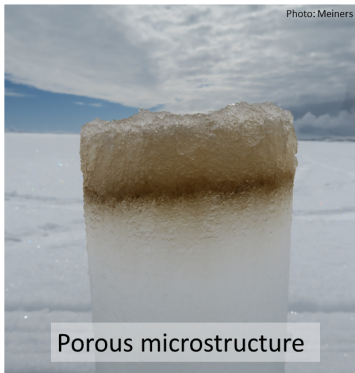
Horvat, Rees Jones, Iams, Schroeder, Flocco, Feltham, *Science Advances* 2017

The effect of melt pond geometry on the distribution of solar energy under first year sea ice

Horvat, Flocco, Rees Jones, Roach, Golden
Geophys. Res. Lett. 2019

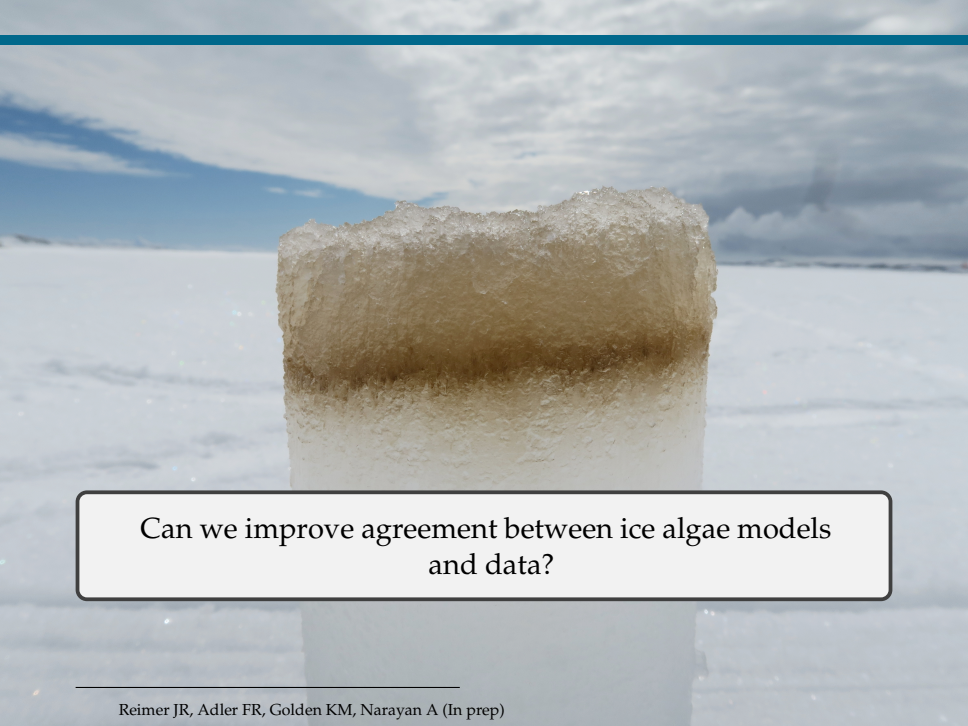
(2015 AMS MRC)

SEA ICE ALGAE



80% of polar bear diet can be traced to ice algae*.

* Brown TA, et al. (2018). *PloS one*, 13(1), e0191631

A vertical ice core sample is shown in the center of the frame. It has a distinct horizontal band of brownish-yellow material, likely ice algae, located in the upper half. The ice is clear and textured. The background is a snowy, flat landscape under a cloudy sky with patches of blue.

Can we improve agreement between ice algae models
and data?

ALGAL BLOOM MODEL*

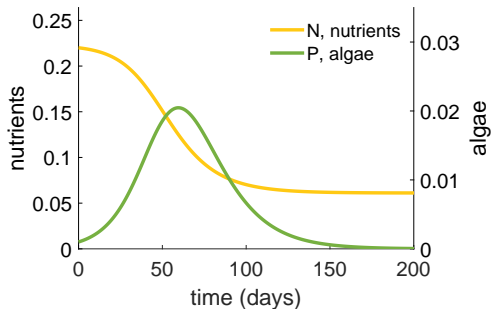
$$\text{nutrients:} \quad \frac{dN}{dt} = \underbrace{\alpha}_{\text{input}} - \underbrace{\beta NP}_{\text{uptake}} - \underbrace{\eta N}_{\text{loss}}$$

$$\text{algae:} \quad \frac{dP}{dt} = \underbrace{\gamma \beta NP}_{\text{growth}} - \underbrace{\delta P}_{\text{death}},$$

$$N(0) = n_0, \quad P(0) = p_0$$

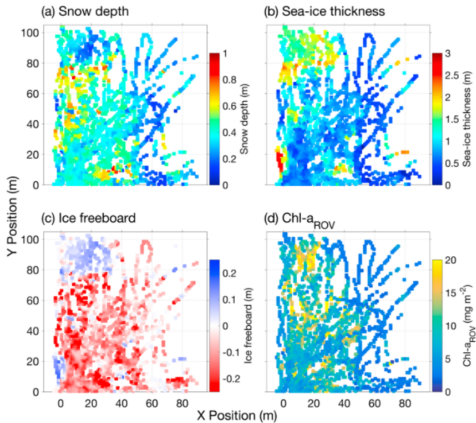
* Huppert, A., et al. (2002). *American Naturalist*, 159(2), 156-171

ALGAL BLOOM MODEL



- poor agreement with data
- poor agreement between models

HETEROGENEITY

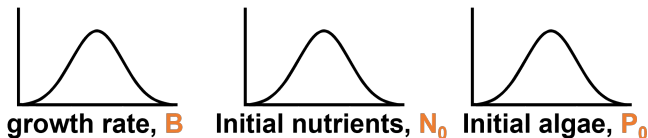


HETEROGENEITY IN INITIAL CONDITIONS

At each location within a larger region, we could consider

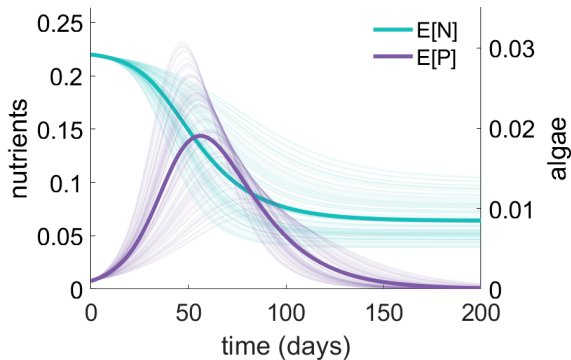
$$\begin{aligned}\frac{dN}{dt} &= \alpha - BNP - \eta N \\ \frac{dP}{dt} &= \gamma BNP - \delta P\end{aligned}$$

$$N(0) = N_0, \quad P(0) = P_0$$



HOW DO WE ANALYZE THIS MODEL?

Monte Carlo simulations?



Too slow! Full algae model takes **8 hours** (cloud computing).

Uncertainty quantification and ecological dynamics in a model of a sea ice algae bloom, in prep. 2022

Jody Reimer, Fred Adler, Ken Golden, and Akil Narayan

POLYNOMIAL CHAOS EXPANSIONS

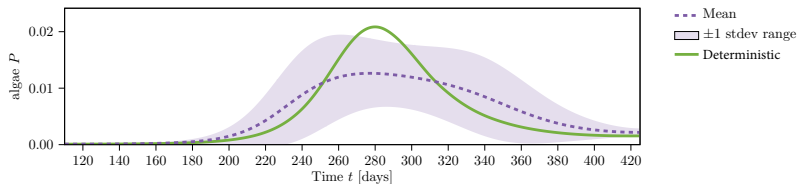
$$N(t; B, P_0, N_0) \approx N_V(t; B, P_0, N_0) := \sum_{j=1}^n \tilde{N}_j(t) \phi_j(B, P_0, N_0),$$

$$P(t; B, P_0, N_0) \approx P_V(t; B, P_0, N_0) := \sum_{j=1}^n \tilde{P}_j(t) \phi_j(B, P_0, N_0),$$

where

- $V := \text{span}\{\phi_j\}_{j=1}^n$
- ϕ_j are orthogonal polynomials that form a basis for V
- $(\tilde{N}_j, \tilde{P}_j)$ need to be computed

ECOLOGICAL INSIGHTS



- lower peak bloom intensity
- longer bloom duration
- able to compare variance to data

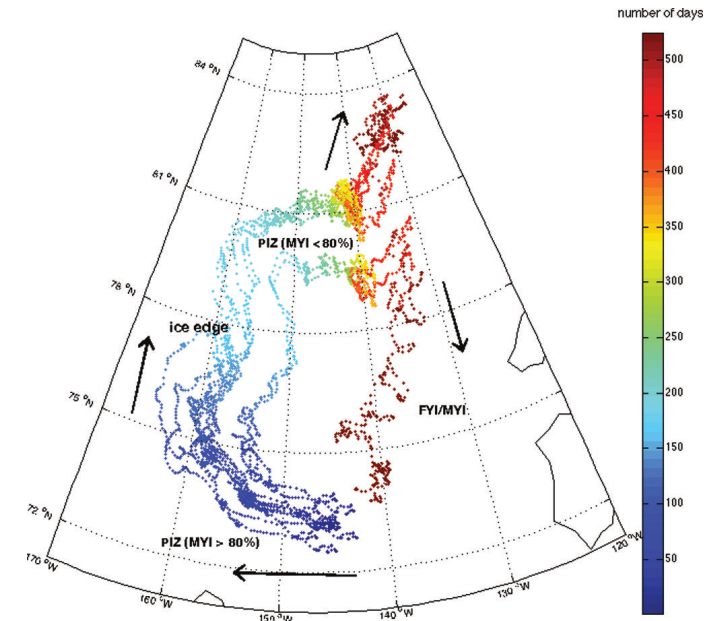
macroscale

Anomalous diffusion in sea ice dynamics

Ice floe diffusion in winds and currents

observations from GPS data:

Jennifer Lukovich, Jennifer Hutchings,
David Barber, *Ann. Glac.* 2015



- On short time scales floes observed (buoy data) to exhibit Brownian-like behavior, but they are also being advected by winds and currents.
- Effective behavior is purely diffusive, sub-diffusive or super-diffusive depending on ice pack and advective conditions - **Hurst exponent**.

modeling:

Huy Dinh, Ben Murphy, Elena Cherkaev,
Court Strong, Ken Golden 2022

floe scale model to analyze transport regimes in
terms of ice pack crowding, advective conditions

Delaney Mosier, Jennifer Hutchings, Jennifer Lukovich,
Marta D'Elia, George Karniadakis, Ken Golden 2022

learning fractional PDE
governing diffusion from data

Floe Scale Model of Anomalous Diffusion in Sea Ice Dynamics

Huy Dinh, Ben Murphy, Elena Cherkaev, Court Strong, Ken Golden 2022

$$\langle |\mathbf{x}(t) - \mathbf{x}(0) - \langle \mathbf{x}(t) - \mathbf{x}(0) \rangle|^2 \rangle \sim t^\alpha$$

α = Hurst exponent

diffusive $\alpha = 1$
sub-diffusive $\alpha < 1$
super-diffusive $\alpha > 1$

Model Approximations

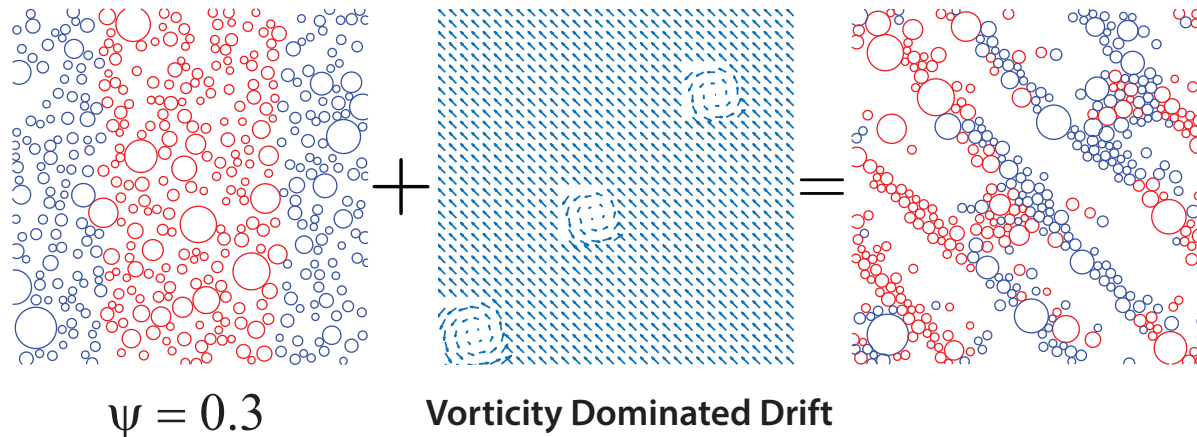
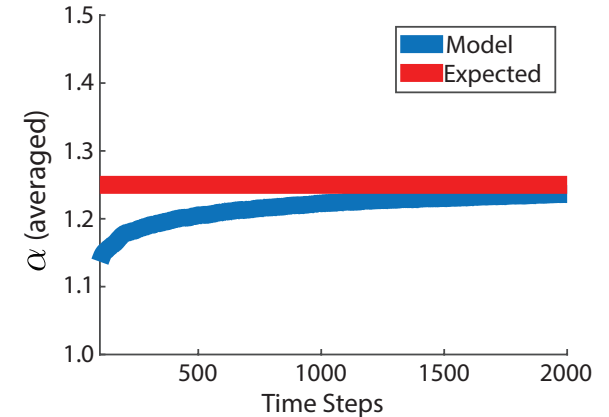
Power Law Size Distribution: $N(D) \sim D^{-k}$

D. A. Rothrock and A. S. Thorndike Journal of Geophysical Research 1984

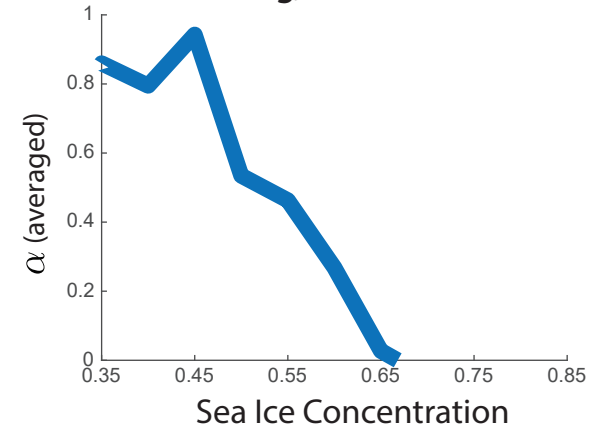
Floe-Floe Interactions: Linear Elastic Collisions

Advective Forcing: Passive, Linear Drag Law

Sparse Packing, Shear Dominated Drift



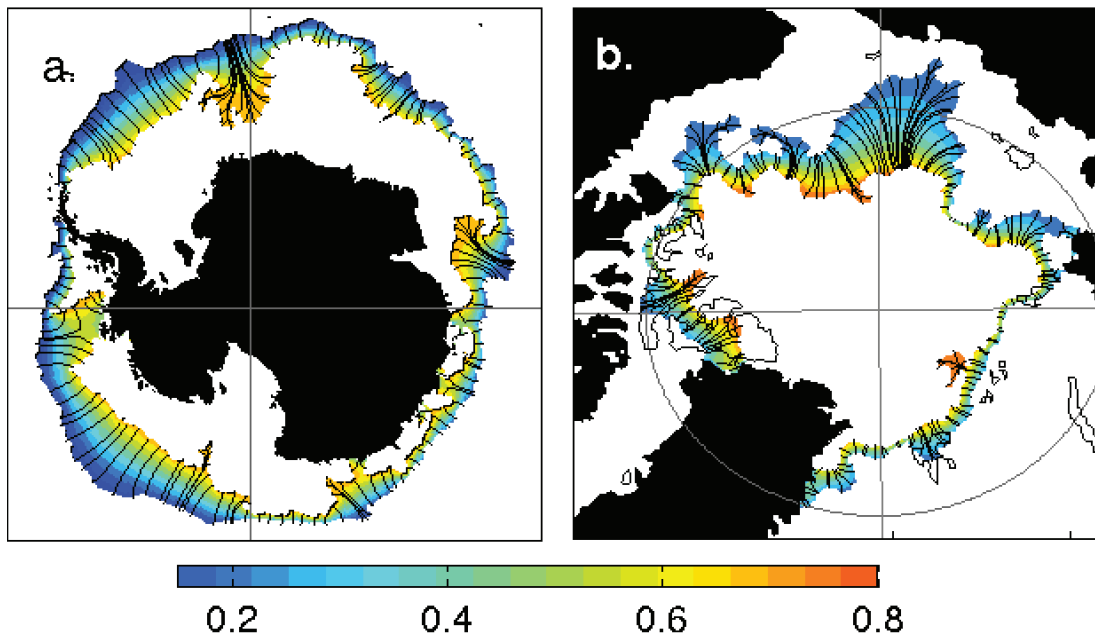
Crowding, Diffusive Drift



Marginal Ice Zone

MIZ

- biologically active region
- intense ocean-sea ice-atmosphere interactions
- region of significant wave-ice interactions



MIZ WIDTH

fundamental length scale of
ecological and climate dynamics

Strong, *Climate Dynamics* 2012

Strong and Rigor, *GRL* 2013

transitional region between
dense interior pack ($c > 80\%$)
sparse outer fringes ($c < 15\%$)

**How to objectively
measure the “width”
of this complex,
non-convex region?**

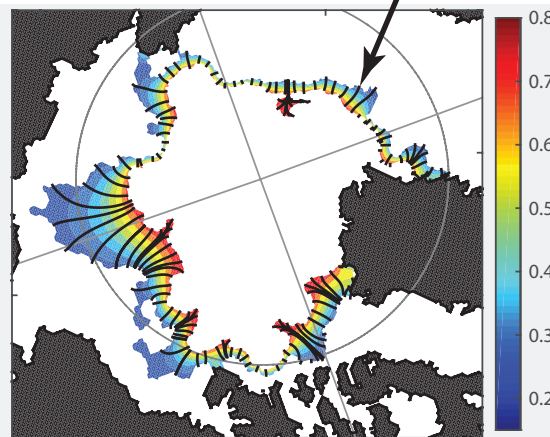
Objective method for measuring MIZ width motivated by medical imaging and diagnostics

Strong, *Climate Dynamics* 2012
Strong and Rigor, *GRL* 2013

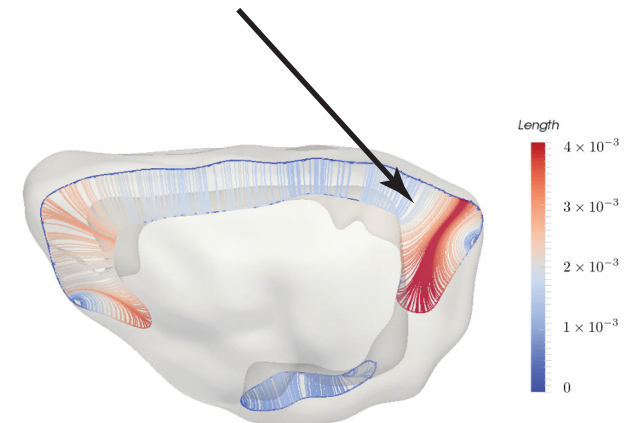
39% widening
1979 - 2012

“average” lengths of streamlines

streamlines of a solution
to Laplace’s equation



Arctic Marginal Ice Zone



**crosssection of the
cerebral cortex of a rodent brain**

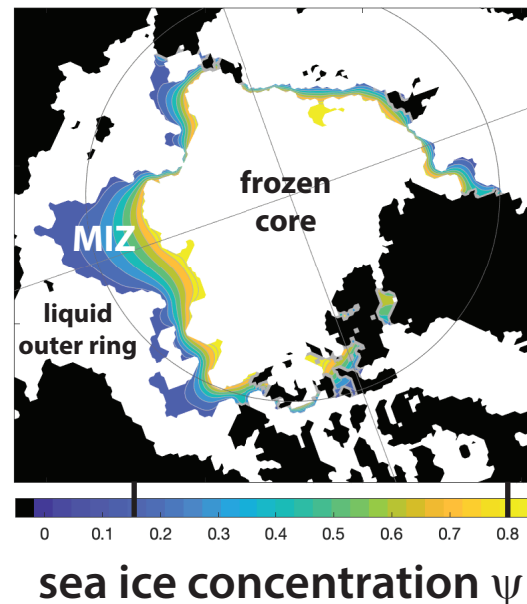
analysis of different MIZ WIDTH definitions

Strong, Foster, Cherkaev, Eisenman, Golden
J. Atmos. Oceanic Tech. 2017

Strong and Golden
Society for Industrial and Applied Mathematics News, April 2017

Model larger scale effective behavior
with partial differential equations that
homogenize complex local structure and dynamics.

Arctic MIZ



Predict MIZ width and location with basin-scale phase change model.
dynamic transitional region - mushy layer - separating two “pure” phases
seasonal and long term trends

C. Strong, E. Cherkaev, and K. M. Golden,
Annual cycle of Arctic marginal ice zone location
and width explained by phase change front model, 2022

MIZ as a moving phase transition region

$$\rho c \frac{\partial T}{\partial t} = \nabla \cdot (k \nabla T) + S$$

$$S = [\rho(c_l - c_s)T + \rho L] \frac{\partial \psi}{\partial t}$$

$$\psi = 1 - \left(\frac{T - T_s}{T_l - T_s} \right)^\alpha$$

$$k_x = \left(\frac{\psi}{k_s} + \frac{1 - \psi}{k_l} \right)^{-1}$$

$$k_z = \psi k_s + (1 - \psi) k_l$$

homogenization

ρ effective density

T temperature

c specific heat

L latent heat of fusion

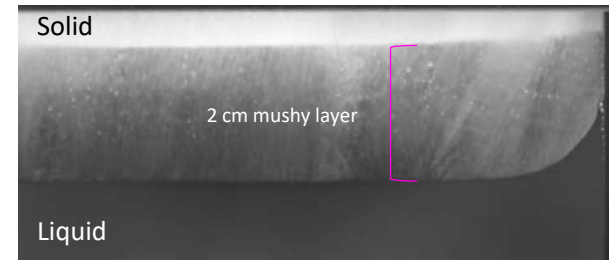
S models nonlinear phase change

ψ sea ice concentration

k effective diffusivity

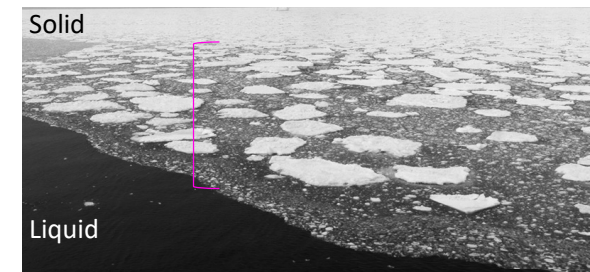
l liquid, s solid

Classical small-scale application



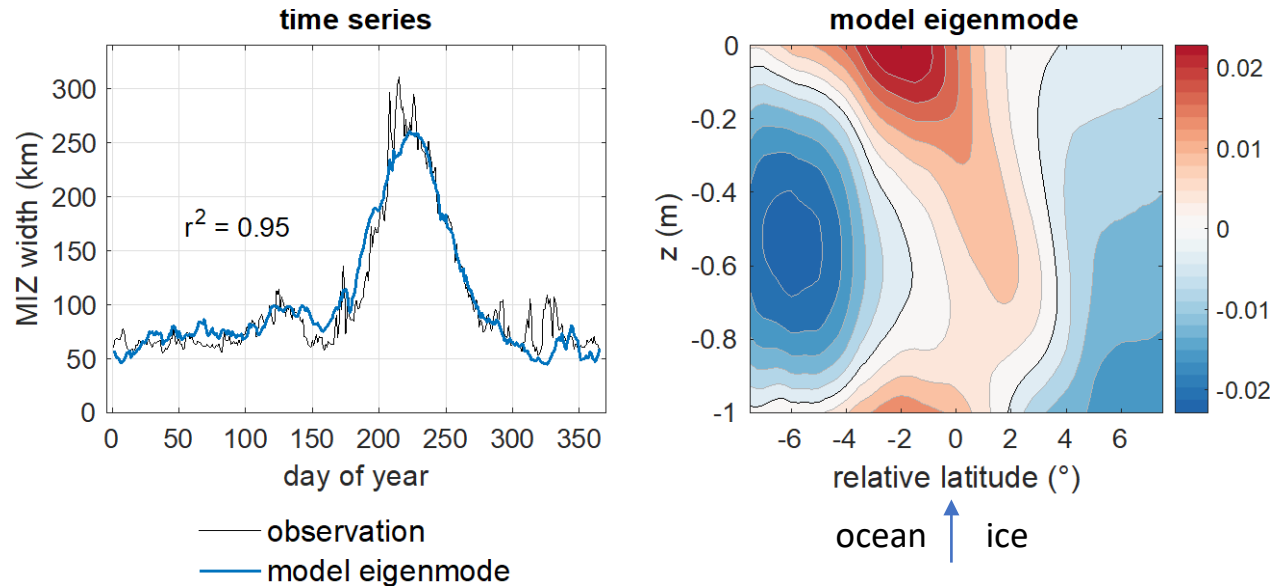
NaCl-H₂O in lab
(Peppin et al., 2007; J. Fluid Mech.)

Macroscale application



- Develop multiscale PDE model for simulating phase transition fronts to predict MIZ seasonal cycles and decadal trends
- Model simulates MIZ as a large-scale mushy layer with effective thermal conductivity derived from physics of composite materials

Model captures basic physics of MIZ dynamics



- Eigenmodes of temperature solution skillfully capture seasonal cycle of MIZ location and width.
- Eigenmode explaining MIZ width captures heat flux convergence into the MIZ layer from atmosphere above and oceanic mixed layer below.
- Model could ultimately be used to explain long term trends toward a wider and more poleward MIZ. Develop more sophisticated homogenization calculations; explore forcing scenarios and how to “drive” MIZ dynamics

Learning the velocity field in an advection diffusion model for sea ice concentration

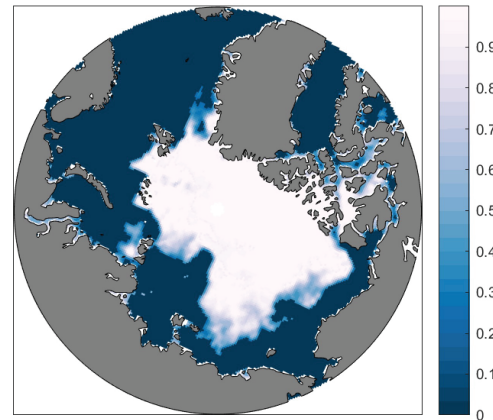
Eric Brown, Delaney Mosier, Bao Wang, Ken Golden, 2022

Goal: Develop PDE model to describe evolution of sea ice concentration field.

advection diffusion model for sea ice concentration:

$$\frac{\partial \psi}{\partial t} = -\mathbf{v} \cdot \nabla \psi + k \Delta \psi$$

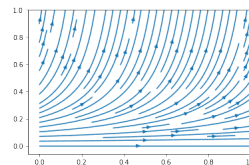
Use two-layer neural network to **infer advective fields** based on satellite imagery



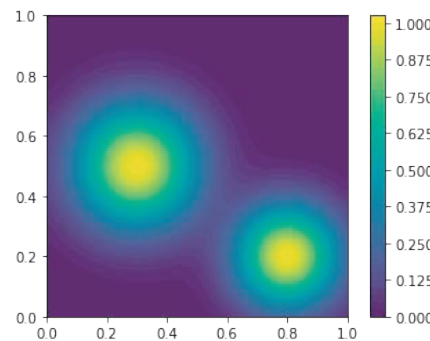
National Snow and Ice Data Center

discretized satellite concentration data

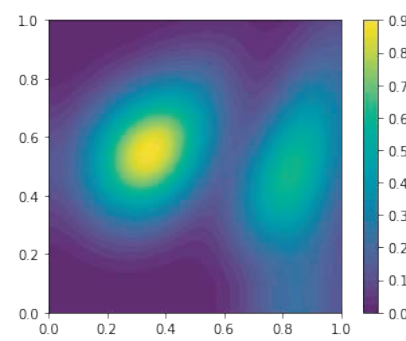
Figure 1. Arctic sea ice concentration in early August 2012.



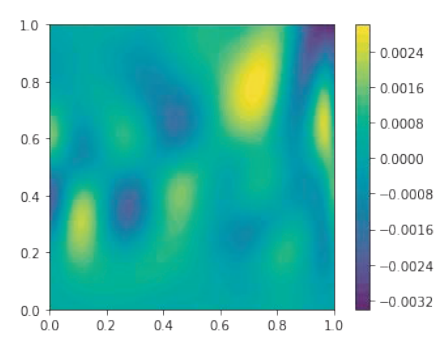
learned velocity



initital test concentration



predicted concentration



error

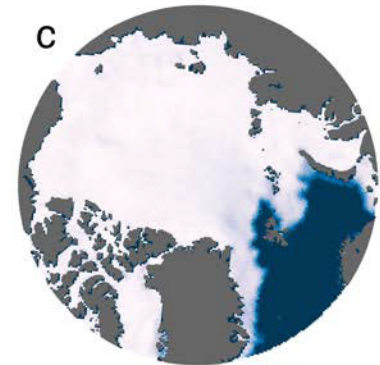
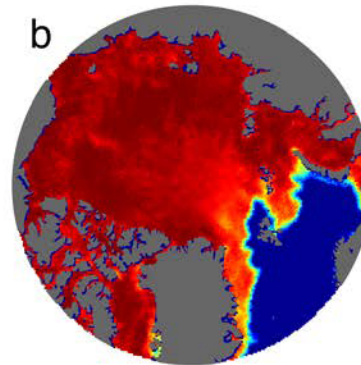
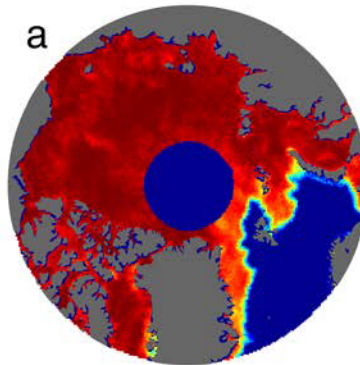
2.5% absolute error in preliminary study

Filling the polar data gap with partial differential equations

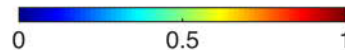
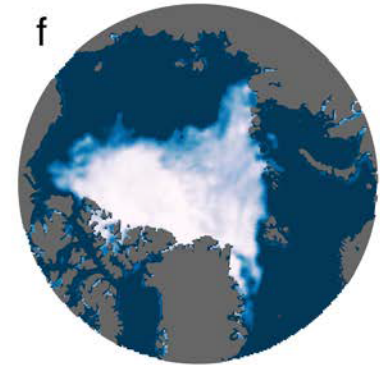
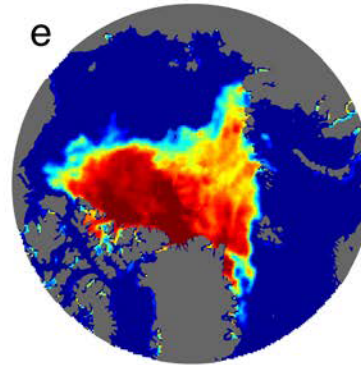
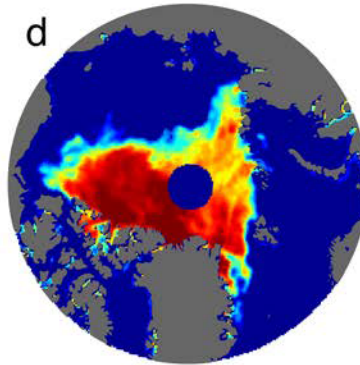
hole in satellite coverage
of sea ice concentration field

previously assumed
ice covered

Gap radius: 611 km
06 January 1985



Gap radius: 311 km
30 August 2007



$$\Delta\psi=0$$

fill = harmonic function with
learned stochastic term

Strong and Golden, *Remote Sensing* 2016
Strong and Golden, *SIAM News* 2017

NOAA/NSIDC Sea Ice Concentration CDR
product update will use our PDE method.

Conclusions

1. Sea ice is a fascinating multiscale composite with structure similar to many other natural and man-made materials.
2. Mathematical methods developed for sea ice advance theories of composites and inverse problems in science and engineering.
3. **Homogenization and statistical physics help *link scales in sea ice and composites***; provide rigorous methods for finding effective behavior; advance sea ice representations in climate models.
4. **Inverse problems of many types** arise naturally in studying sea ice and the impact of climate change in Earth's polar regions.
5. Field experiments are essential to developing relevant mathematics.
6. Our research is helping to **improve projections of climate change**, the fate of Earth's sea ice packs, and the ecosystems they support.

University of Utah Sea Ice Modeling Group (2017-2021)

Senior Personnel: Ken Golden, Distinguished Professor of Mathematics
Elena Cherkaev, Professor of Mathematics
Court Strong, Associate Professor of Atmospheric Sciences
Ben Murphy, Adjunct Assistant Professor of Mathematics

Postdoctoral Researchers: Noa Kraitzman (now at ANU), Jody Reimer

Graduate Students: Kyle Steffen (now at UT Austin with Clint Dawson)
Christian Sampson (now at UNC Chapel Hill with Chris Jones)
Huy Dinh (now a sea ice MURI Postdoc at NYU/Courant)
Rebecca Hardenbrook
David Morison (Physics Department)
Ryleigh Moore
Delaney Mosier
Daniel Hallman

Undergraduate Students: Kenzie McLean, Jacqueline Cinella Rich,
Dane Gollero, Samir Suthar, Anna Hyde,
Kitsel Lusted, Ruby Bowers, Kimball Johnston,
Jerry Zhang, Nash Ward, David Gluckman

High School Students: Jeremiah Chapman, Titus Quah, Dylan Webb

Sea Ice Ecology Group Postdoc Jody Reimer, Grad Student Julie Sherman,
Undergraduates Kayla Stewart, Nicole Forrester



ISSN 0002-9920 (print)
ISSN 1088-9477 (online)

Notices

of the American Mathematical Society

November 2020

Volume 67, Number 10



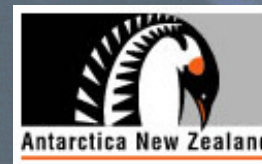
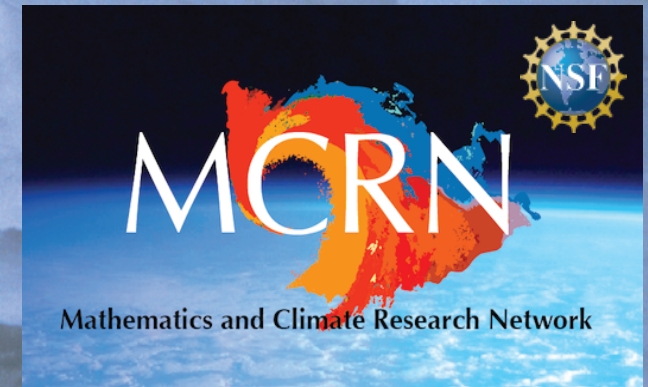
THANK YOU

Office of Naval Research

Applied and Computational Analysis Program
Arctic and Global Prediction Program

National Science Foundation

Division of Mathematical Sciences
Division of Polar Programs



Buchanan Bay, Antarctica Mertz Glacier Polynya Experiment July 1999

Modeling Sea Ice



*Kenneth M. Golden, Luke G. Bennetts,
Elena Cherkaev, Ian Eisenman, Daniel Feltham,
Christopher Horvat, Elizabeth Hunke,
Christopher Jones, Donald K. Perovich,
Pedro Ponte-Castañeda, Courtenay Strong,
Deborah Sulsky, and Andrew J. Wells*

Kenneth M. Golden is a Distinguished Professor of Mathematics at the University of Utah. His email address is golden@math.utah.edu.

Luke G. Bennetts is an associate professor of applied mathematics at the University of Adelaide. His email address is luke.bennetts@adelaide.edu.au.

Elena Cherkaev is a professor of mathematics at the University of Utah. Her email address is elena@math.utah.edu.

Ian Eisenman is an associate professor of climate, atmospheric science, and physical oceanography at the Scripps Institution of Oceanography at the University of California San Diego. His email address is eisenman@ucsd.edu.

Daniel Feltham is a professor of climate physics at the University of Reading. His email address is d.l.feltham@reading.ac.uk.

Christopher Horvat is a NOAA Climate and Global Change Postdoctoral Fellow at the Institute at Brown for Environment and Society at Brown University. His email address is christopher_horvat@brown.edu.

Elizabeth Hunke is a deputy group leader, T-3 fluid dynamics and solid mechanics group at the Los Alamos National Laboratory. Her email address is elclare@lanl.gov.

Christopher Jones is a Bill Guthridge Distinguished Professor of Mathematics

at the University of North Carolina, Chapel Hill. His email address is ckrtj@unc.edu.

Donald K. Perovich is a professor of engineering at the Thayer School of Engineering at Dartmouth College. His email address is donald.k.perovich@dartmouth.edu.

Pedro Ponte-Castañeda is a Raymond S. Markowitz Faculty Fellow and professor of mechanical engineering and applied mechanics and of mathematics at the University of Pennsylvania. His email address is ponte@seas.upenn.edu.

Courtenay Strong is an associate professor of atmospheric sciences at the University of Utah. His email address is court.strong@utah.edu.

Deborah Sulsky is a professor of mathematics and statistics and of mechanical engineering at the University of New Mexico. Her email address is sulsky@math.unm.edu.

Andrew J. Wells is an associate professor of physical climate science at the University of Oxford. His email address is Andrew.Wells@physics.ox.ac.uk.

Communicated by Notices Associate Editor Reza Malek-Madani.

*For permission to reprint this article, please contact:
reprint-permission@ams.org.*

Fire endangers Hobart's ice ship

By DAVID CARRIGG

AN engine-room fire has left the Hobart-based Antarctic research ship *Aurora Australis* without power in dangerous sea ice off the Antarctic coast.

None of the 79 people on board was injured in the blaze, which broke out early yesterday morning while the ship was in deep water 185km off the coast.

The extent of the damage is not known.

Australian Antarctic Division director Rex Moncur said the fire was extinguished by flooding the engine room with an inert gas.

The gas had to be cleared before crew wearing breathing apparatus could enter and assess the situation.

He said it could be some time before the extent of damage was known.

The 25 crew and 54 expeditioners, mostly from Hobart, would wear thermal clothing and stay below decks to keep warm.

"There is always a risk of becoming ice-bound in these waters at this time of the year but at this stage we don't expect to launch a rescue mission from Hobart," Mr Moncur said.

The ship was in regular radio contact with the Antarctic Div-



A file photo of the *Aurora Australis* in Antarctica.

ision's Hobart office.

He expected the expeditioners and crew to abandon the pioneering winter voyage and return the ship to Hobart for repairs in about a week.

The Antarctic Division, which hires the ship from P&O Australia, would not be hiring another vessel for the expedition.

"It's a pretty specialist vessel so you couldn't get the sort of research capability that this ship has got readily available," Mr Moncur said.

"We hope the next voyage can still proceed on schedule, which is early September."

The *Aurora Australis* is owned by P&O Australia and chartered by the Antarctic Div-

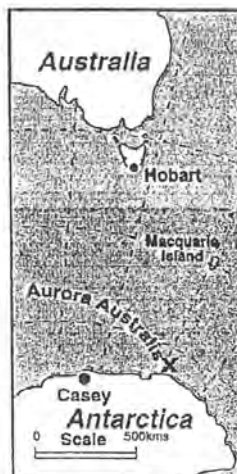
ision for about \$11 million a year.

P&O Australia managing director Richard Hein said yesterday the company was assessing the situation and a number of rescue options were being considered.

It was too early to say whether P&O would be liable for the cost of the aborted mission.

The vessel left Hobart last Wednesday for a seven-week voyage mainly to study a polynya, an area where savage winds break up the sea ice and cause heavy, salt-laden water to sink to the bottom.

The ship was nearing the polynya when the fire broke out.



Oceanographers believe a closer study of the phenomenon will lead to a better understanding of climate change.

CSIRO Marine Research oceanographer Steve Rintoul said the dense bottom water, created only in a few places in Antarctica and to a lesser extent in the North Atlantic, was critical to the chemistry and biology of the world's oceans.

Fire strands Antarctic ship in sea ice

AN engine room fire has disabled the icebreaker *Aurora Australis* in sea ice, deep in Antarctic waters.

There were no injuries and the ship was not in danger after Tuesday night's fire.

Australian Antarctic Division director Mr Rex Moncur said. But Mr Moncur said he expected it would have to abandon its pioneering mid-winter voyage to the edge of the Ant-

arctic continent and return to Hobart for repairs.

The cause of the fire was not known but the engines have been turned off, with the ship 100 nautical miles from the Antarctic coast.

THE CANBERRA TIMES

Thursday 23 July 1998

Page 4

Antarctic voyage stopped by fire

HOBART: An engine room fire has disabled the Australian icebreaker *Aurora Australis* in sea ice, deep in Antarctic waters.

Australian Antarctic Division director Rex Moncur said there were no injuries and the ship was not in danger after Tuesday night's fire.

But Mr Moncur said he expected *Aurora Australis* would have to abandon its pioneering mid-winter voyage to the edge of the Antarctic continent to return to Hobart for repairs.

The fire had been extinguished and the engines were turned off, leaving the ship in sea ice about 100 nautical miles from the Antarctic coast, he said. The weather was good.

Crew had to wear breathing apparatus to enter the engine room and it was likely to be 24 hours before the damage could be fully assessed.

The *Aurora*, with 54 expeditioners and 25 crew, left Hobart last Wednesday for a seven-week voyage which was to have focused on a polynya, an area where savage winds break up the sea ice and cause heavy, salt-laden water to sink to the bottom.

Mr Moncur said, the cause of the fire was not yet known.

2:45 am July 22, 1998

"Please don't be alarmed but we have an uncontrolled fire in the engine room"

about 10 minutes later ...

"Please don't be alarmed but we're lowering the lifeboats"

Sydney Morning Herald
23 July, 1998

ICEBREAKER BURNS

A pioneering \$2-million Australian scientific voyage to the mid-winter Antarctic polynya is expected to be scrapped following an engine room fire on the *Aurora Australis* yesterday. The 54 people on board were forced on deck in the

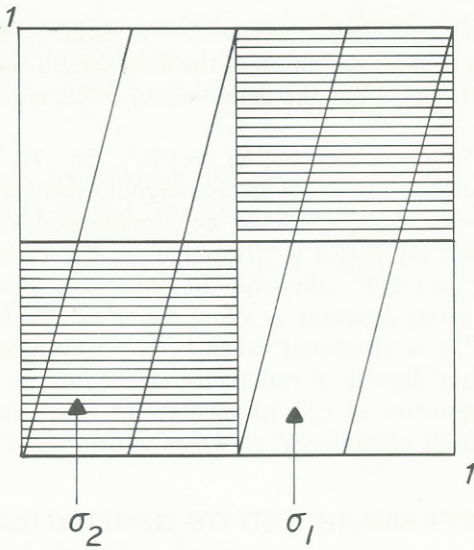


Classical transport in quasiperiodic media

Golden, Goldstein, and Lebowitz

Phys. Rev. Lett. 1985

J. Stat. Phys. 1990



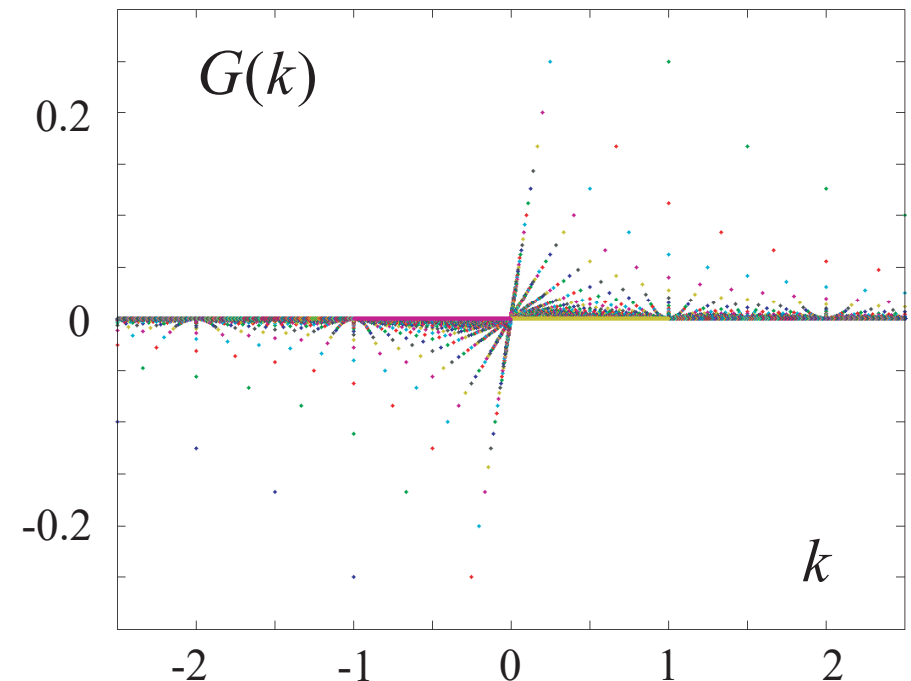
line of slope k through
an infinite checkerboard

effective conductivity $\sigma^*(k)$

effective resistivity $1/\sigma^*(k) = 1 - G(k)$

$$G(k) = \begin{cases} 0, & k \text{ irrational} \\ 1/pq, & k = p/q \text{ rational} \end{cases}$$

continuous at k irrational
discontinuous at k rational



Special Issue on the Mathematics of Planet Earth

Read about the application of mathematics and computational science to issues concerning invasive populations, Arctic sea ice, insect flight, and more in this Planet Earth **special issue!**

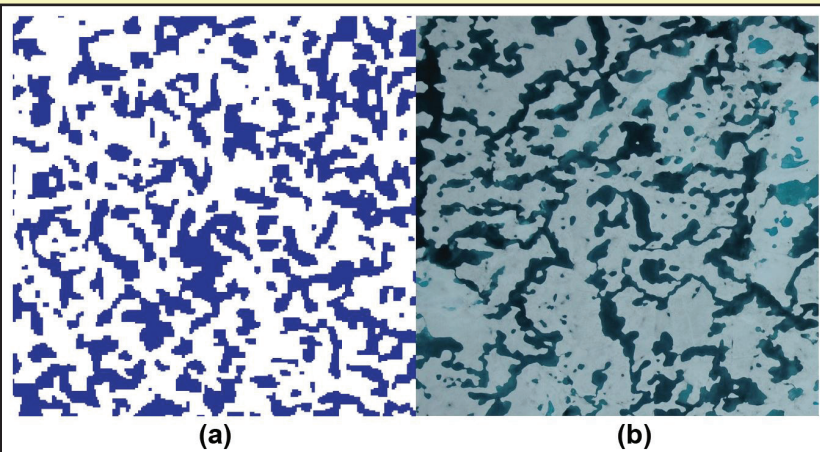


Figure 3. Comparison of real Arctic melt ponds with metastable equilibria in our melt pond Ising model. **3a.** Ising model simulation. **3b.** Real melt pond photo. Figure 3a courtesy of Yiping Ma, 3b courtesy of Donald Perovich.

Vast labyrinthine ponds on the surface of melting Arctic sea ice are key players in the polar climate system and upper ocean ecology. Researchers have adapted the Ising model, which was originally developed to understand magnetic materials, to study the geometry of meltwater's distribution over the sea ice surface. In an article on page 5, Kenneth Golden, Yiping Ma, Courtenay Strong, and Ivan Sudakov explore model predictions.

Controlling Invasive Populations in Rivers

By Yu Jin and Suzanne Lenhart

Flow regimes can change significantly over time and space and strongly impact all levels of river biodiversity, from the individual to the ecosystem. Invasive species in rivers—such as bighead and silver carp, as well as quagga and zebra mussels—continue to cause damage. Management of these species may include targeted adjustment of flow rates in rivers, based on recent research that examines the effects of river morphology and water flow on rivers' ecological statuses. While many previous methodologies rely on habitat suitability models or oversimplification of the hydrodynamics, few studies have focused on the integration of ecological dynamics into water flow assessments.

Earlier work yielded a hybrid modeling approach that directly links river hydrology with stream population models [3]. The hybrid model's hydrodynamic component is based on the water depth in a gradually varying river structure. The model derives the steady advective flow from this structure and relates it to flow features like water discharge, depth, velocity, cross-

sectional area, bottom roughness, bottom slope, and gravitational acceleration. This approach facilitates both theoretical understanding and the generation of quantitative predictions, thus providing a way for scientists to analyze the effects of river fluctuations on population processes.

When a population spreads longitudinally in a one-dimensional (1D) river with spatial heterogeneities in habitat and temporal fluctuations in discharge, the resulting hydrodynamic population model is

$$N_t = -A_t(x, t) \frac{N}{A(x, t)} + \frac{1}{A(x, t)} \left(D(x, t) A(x, t) N_x \right)_x - \frac{Q(t)}{A(x, t)} N_x + rN \left(1 - \frac{N}{K} \right)$$

$$\begin{aligned} N(0, t) &= 0 & \text{on } (0, T), x = 0, \\ N_x(L, t) &= 0 & \text{on } (0, T), x = L, \\ N(x, 0) &= N_0(x) & \text{on } (0, L), t = 0 \end{aligned}$$

(1)

See **Invasive Populations** on page 4

Modeling Resource Demands and Constraints for COVID-19 Intervention Strategies

By Erin C.S. Acquesta, Walt Beyeler, Pat Finley, Katherine Klise, Monear Makvandi, and Emma Stanislawski

As the world desperately attempts to control the spread of COVID-19, the need for a model that accounts for realistic trade-offs between time, resources, and corresponding epidemiological implications is apparent. Some early mathematical models of the outbreak compared trade-offs for non-pharmaceutical interventions [3], while others derived the necessary level of test coverage for case-based interventions [4] and demonstrated the value of prioritized testing for close contacts [7].

Isolated analyses provide valuable insights, but real-world intervention strategies are interconnected. Contact tracing is the lynchpin of infection control [6] and forms the basis of prioritized testing. Therefore, quantifying the effectiveness of contact tracing is crucial to understanding the real-life implications of disease control strategies.

Contact Tracing Demands

Contact tracers are skilled, culturally competent interviewers who apply their knowledge of disease and risk factors when notifying people who have come into contact with COVID-19-infected individuals. They also continue to monitor the situation after case investigations [1].

Case investigation consists of four steps:

1. Identify and notify cases
2. Interview cases
3. Locate and notify contacts
4. Monitor contacts.

Most health departments are implementing case investigation, contact identification, and quarantine to disrupt COVID-19 transmission. The timeliness of contact tracing is constrained by the length of the infectious period, the turn-around time for testing and result reporting, and the ability to successfully reach and interview patients and their contacts. The European Centre for Disease Prevention and Control approximates that contact tracers spend one to two hours conducting an interview [2]. Estimates regarding the timelines of other steps are limited to subject matter expert elicitation and can vary based on cases' access to phone service or willingness to participate in interviews.

Bounded Exponential

The fundamental structure of our model follows traditional susceptible-exposed-infected-recovered (SEIR) compartmental modeling [5]. We add an asymptomatic population A , a hospitalized population H , and disease-related deaths D , as well as corresponding quarantine states. We define the states $\{S_i, E_i, A_i, I_i, H, R, D\}_{i=0,1}$ for our compartments, such that $i=0$ and $i=1$

correspond to unquarantined and quarantined respectively. Rather than focus on the dynamics that are associated with the state transition diagram in Figure 1, we introduce a formulation for the real-time demands on contact tracers' time as a function of infection prevalence, while also respecting constraints on resources.

When the work that is required to investigate new cases and monitor existing contacts exceeds available resources, a backlog develops. To simulate this backlog, we introduce a new compartment C for tracking the dynamic states of cases:

$$\frac{dC}{dt} = [flow_{in}] - [flow_{out}].$$

Flow into the backlog compartment, represented by $[flow_{in}]$, reflects case identification that is associated with the following transitions in the model:

- The rate of random testing: $q_{rA}(t)A_0(t) \rightarrow A_1(t)$ and $q_{rI}(t)I_0(t) \rightarrow I_1(t)$
- Testing triggered by contact tracing: $q_{tA}(t)A_0(t) \rightarrow A_1(t)$, $q_{tI}(t)I_0(t) \rightarrow I_1(t)$, and $q_{tE}(t)E_i(t) \rightarrow \{A_i(t), I_i(t)\}$
- The population that was missed by the non-pharmaceutical interventions that require hospitalization: $\tau_{IH}(t)I_0(t) \rightarrow H(t)$.

Here, $q_{rs}(t)$ defines the time-dependent rate of random testing, $q_{ts}(t)$ signifies the time-dependent rate of testing that is triggered by contact tracing, and τ_{IH} is the inverse of the expected amount of time for which an infected individual is symptomatic before hospitalization. These terms collectively provide the simulated number of newly-identified positive COVID-19 cases. However, we also need the average number of contacts per case. We thus define function $\mathcal{K}(\kappa, T_s, \phi_\kappa)$ that depends on the average number of contacts a day (κ), the average number of days for which an individual is infectious before going into isolation (T_s), and the likelihood that the individual

See **COVID-19 Intervention** on page 3

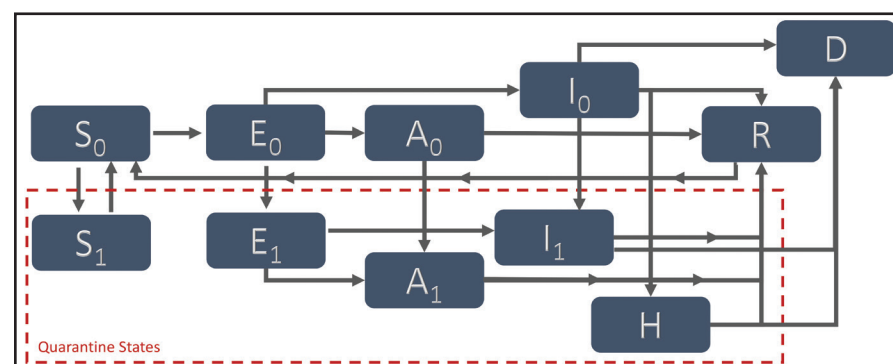


Figure 1. Disease state diagram for the compartmental infectious disease model. Figure courtesy of the authors.

Nonprofit Org
U.S. Postage
PAID
Permit No 360
Bellmawr, NJ

siam
SOCIETY for INDUSTRIAL and APPLIED MATHEMATICS
3600 Market Street, 6th Floor
Philadelphia, PA 19104-2688 USA

How do scales interact in the sea ice system?

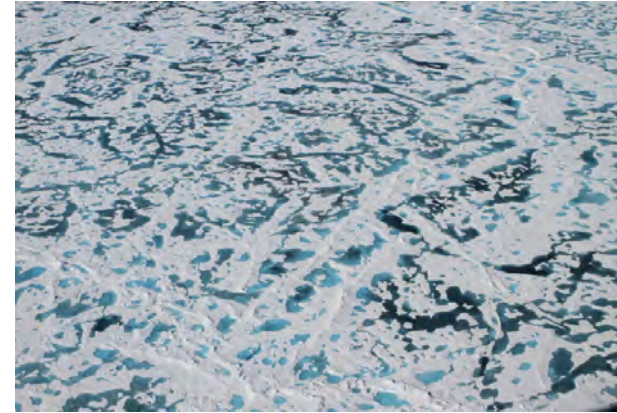
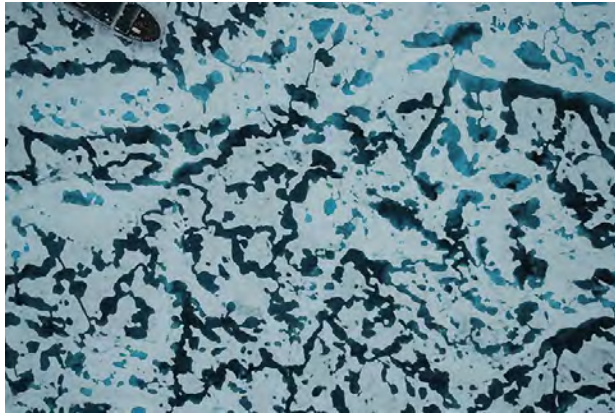


basin scale -
grid scale
albedo

NASA

Linking Scales

km
scale
melt
ponds

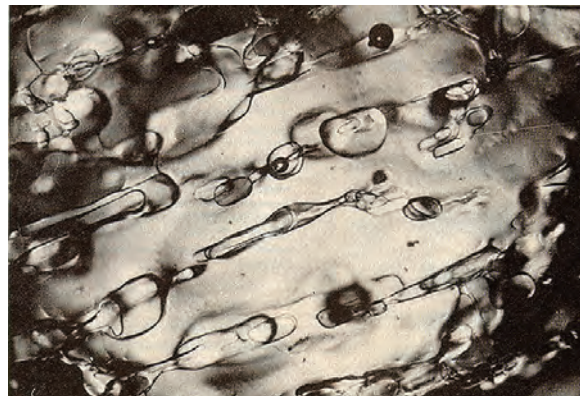


Perovich

Linking

Scales

mm
scale
brine
inclusions



meter
scale
snow
topography

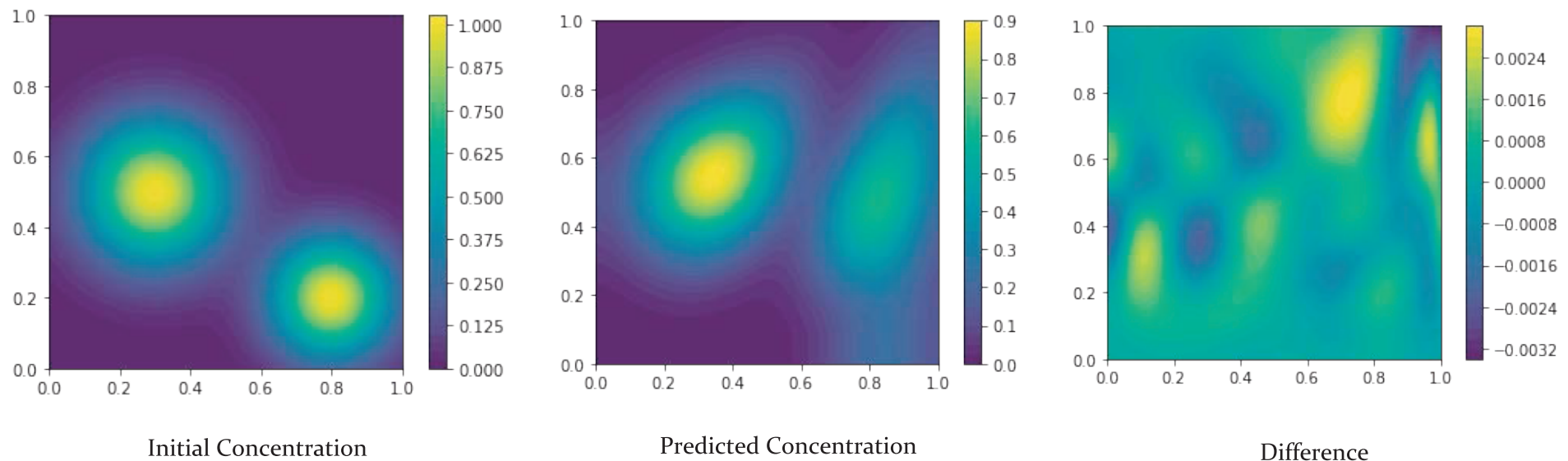
Learning the Velocity Field (cont.)

Method:

1. Parameterize velocity field with a two-layer **neural network**, N , to obtain:

$$\psi_t = N(x, y, \theta, t) \cdot \nabla \psi + k \Delta \psi$$

2. Use FEM to solve and the adjoint method to select optimal parameters
3. Repeat this process to train the model and arrive at approximate velocity field
4. Predict concentration at future time steps (**2.5% absolute error** in preliminary study)



Stieltjes Integral Representation for Complex Viscoelasticity

homogenized

$$\langle \sigma_{ij} \rangle = C_{ijkl}^* \langle \epsilon_{kl} \rangle$$

local

$$\nabla \cdot \sigma = 0$$

$$\sigma_{ij} = C_{ijkl} \epsilon_{kl}$$

Strain Field

$$C_{ijkl} = (v_1 \chi + (1 - \chi) v_2) \lambda_s$$

$$\epsilon = \frac{1}{2} [\nabla u + (\nabla u)^T] = \nabla^s u$$

$$\nabla \cdot ((v_1 \chi + (1 - \chi) v_2) \lambda_s : \epsilon) = 0$$

$$\epsilon = \epsilon_0 + \epsilon_f \text{ where } \epsilon_f = \nabla^s \phi$$

$$s = \frac{1}{1 - \frac{v_1}{v_2}}$$

Elasticity Tensor

$$C_{ijkl}^* = v^* \left(\delta_{ik} \delta_{jl} + \delta_{il} \delta_{jk} - \frac{2}{3} \delta_{ij} \delta_{kl} \right) = v^* \lambda_s$$

RESOLVENT $\epsilon = \left(1 - \frac{1}{s} \Gamma \chi \right)^{-1} \epsilon_0 \quad \Gamma = \nabla^s (\nabla \cdot \nabla^s)^{-1} \nabla \cdot \quad \epsilon_0 \text{ avg strain}$

$$F(s) = 1 - \frac{v^*}{v_2}$$

$$F(s) = ||\epsilon_0||^{-2} \int_{\Sigma} \frac{d\mu(\lambda)}{s - \lambda}$$